A comparison between the stability field of a Cl-rich scapolite at elevated pressures and the end-member marialite

Kaléo M. F. Almeida[1*]

David M. Jenkins[1]

[1] Department of Geological Sciences and Environmental Studies

Binghamton University

Binghamton, NY, 13902

[*]Corresponding author

Abstract

Scapolites are pervasive rock-forming aluminousilicates that are found in metamorphic, igneous and metasomatic environments; nonetheless, the stability field of Cl-rich scapolite is not well constrained. This experimental study investigated two reactions involving Cl-rich scapolite. First, the anhydrous reaction (1) of plagioclase + halite + calcite to form scapolite modeled as:

$3(Na_{0.8}Ca_{0.2})(Al_{1.2}Si_{2.8})O_8 + 0.8NaCl + 0.2CaCO_3 = (Na_{3.2}Ca_{0.8})(Al_{3.6}Si_{8.4})O_{24}(Cl_{0.8}(CO_3)_{0.2})$

plagioclase ($Ab_{80}An_{20}$) halite calcite scapolite($Ma_{80}Me_{20}$)

was investigated to determine the effect of the Ca-rich meionite (Me = $Ca_4Al_6Si_6O_{24}CO_3$) component on the Na end-member marialite (Ma = $Na_4Al_3Si_9O_{24}Cl$). Second, the effect of water on this reaction was investigated using the hydrothermally equivalent reaction (2) H_2O + scapolite ($Ma_{80}Me_{20}$) = 3 plagioclase ($Ab_{80}An_{20}$) + $CaCO_3$ + liquid, where the liquid is assumed to be a saline-rich hydrous-silicate melt. Experiments were investigated with synthetic phases over the range of 500-1030 °C and 0.4-2.0 GPa. For reaction (1), intermediate composition scapolite shows a wide thermal stability and is stable relative to plagioclase + halite + calcite at temperatures above 750 °C at 0.4 GPa and 760 °C at 2.0 GPa. For reaction (2), intermediate scapolite appears to be quite tolerant to water; it forms at a minimum bulk salinity [X_{NaCl} = molar ratio of NaCl/(NaCl + H_2O)] of the brine of approximately 0.2 X_{NaCl} at 830 °C and 680 °C at pressures of 2.0 GPa and 1.5 GPa, respectively. Based on a study done by Almeida and Jenkins (2017), pure marialite is very intolerant to water when compared to intermediate composition scapolite. Compositional changes in the scapolite and plagioclase were characterized by X-ray diffraction and electron microprobe analysis and found to shift from the nominal bulk compositions to the observed compositions of $Ma_{85}Me_{15}$ for scapolite and to $Ab_{91}An_{09}$ for plagioclase. These results were used to model the phase equilibria along the marialite-meionite

join in temperature-composition space. This study demonstrates that a small change in the scapolite composition from end-member marialite to $Ma_{85}Me_{15}$ expands the stability field of marialite significantly, presumably due to the high entropy of mixing in scapolite, as well as increases its tolerance to water. This supports the much more common presence of intermediate scapolites in hydrothermal settings than either end-member meionite or marialite as is widely reported in the literature.

Keywords: scapolite, marialite, meionite, solid solution, chlorine, chloride brine, plagioclase

Introduction

The scapolite mineral group is a widespread rock-forming aluminosilicate and it is reported extensively in nature over a wide range of solid solution. The general formula of scapolite can be illustrated as $M_4T_{12}O_{24}A$, where the major components are M = Na and Ca, T = Si and Al, and A = Cl, CO_3, and SO_4. Minerals in the scapolite group can be regarded as the result of combining three moles of plagioclase with a salt (i.e., NaCl, $CaCO_3$, $CaSO_4$) (e.g., Evans et al., 1969; Goldsmith, 1976; Hassan and Buseck, 1988; Teertstra and Sherriff, 1997). They can be chemically represented as a solid solution of four end-members: a sodium chloride end-member, marialite ($Na_4Al_3Si_9O_{24}Cl$), two calcium carbonate end-members, meionite ($Ca_4Al_6Si_6O_{24}CO_3$) and mizzonite ($NaCa_3Al_5Si_7O_{24}CO_3$), and a calcium sulfate end-member, sulfate meionite or silvialite ($Ca_4Al_6Si_6O_{24}SO_4$) (Newton and Goldsmith, 1976; Teertstra et al. 1999). Unlike other chloride bearing minerals (such as amphiboles, micas, and apatite), scapolite contains little to no OH, thus its chemistry can be used as a tracer of the Cl and CO_2 contents of the fluid responsible for its formation, independently of fH_2O (Ellis, 1978; Rebbert and Rice, 1997; Filiberto et al., 2014).

75 The relative prevalence and abundance of scapolite in metamorphic rocks and
76 hydrothermally altered igneous rocks suggests a rather wide stability field for this mineral group
77 (Goldsmith, 1976; Boivin and Camus, 1981; Vanko and Bishop, 1982; Mora and Valley, 1989;
78 Lieftink et al., 1993; Kullerud and Erambert, 1999; Johnson and Barton, 2000a, 2000b).
79 Interestingly, essentially all of the literature on natural scapolites have something in common: in
80 all cases they are reported as solid solutions. In fact, accounts of naturally occurring scapolites
81 approaching end-members (Cl, CO_3, and SO_4) are rare (e.g., Teertstra and Sherriff, 1997; Vanko
82 and Bishop, 1982; Lieftink et al., 1993; Filiberto et al., 2014), suggesting that the conditions
83 under which end-member scapolites form are rather unusual in nature.
84 Experimental studies reporting stability fields in pressure-temperature (*P*-*T*) space for end-
85 member scapolites are those of Newton and Goldsmith (1976) and Almeida and Jenkins (2017).
86 Newton and Goldsmith (1976) investigated the stability field of end-member meionite and
87 sulfate-meionite in the $CaAl_2Si_2O_8$-$CaCO_3$ and $CaAl_2Si_2O_8$-$CaSO_4$ systems, respectively. These
88 authors found end-member meionite and sulfate meionite to be stable at higher temperatures
89 relative to the anorthite + salt assemblage. They reported that meionite is stable relative to
90 anorthite and calcite above 875 °C, almost independent of pressure. On the contrary, sulfate-
91 meionite appears to have a strong pressure dependency with the boundary located at 1.3 GPa at
92 1000 °C and having a negative d*P*/d*T* slope of -0.0022 GPa/°C, which restricts the conditions of
93 its formation to high pressure (> 0.6 GPa at 1300 °C) environments. This is in agreement with
94 the literature where scapolites with the highest sulfur content tend to come from deep-seated
95 rocks (Lovering and White, 1964; Yoshino and Satish-Kumar, 2001; Hammerli et al., 2017).
96 Although Newton and Goldsmith (1976) tabulated several experiments involving marialite, they
97 did not report a *P*-*T* stability field for it. Based on various observations reported in literature,

Filiberto et al. (2014) proposed a P-T diagram for marialite, however no systematic experimental study was presented for this end-member. Almeida and Jenkins (2017) investigated the *P-T* stability field of end-member marialite in the $NaAlSi_3O_8$-NaCl and $NaAlSiO_3O_8$-NaCl-H_2O systems, for both dry and hydrothermal conditions, respectively. The main conclusions were that marialite (i) requires high-temperatures, equivalent to granulite or ultra-high-temperature (UHT) facies to be stable, and (ii) requires high NaCl concentrations, even going above the saturation level of halite in the H_2O-NaCl system, in order to be stable at hydrothermal conditions. This necessity of a high brine concentration and high temperature to stabilize end-member marialite indicates it is a "dry" mineral, and it would therefore not be likely to have a hydrothermal origin. Similar to sulfate meionite, marialite also appears to require intermediate-to-high pressures to be stable with the lowest pressure where marialite occur occurs being 0.64 GPa at 930 °C (Almeida and Jenkins, 2017). In the presence of a concentrated brine, Almeida and Jenkins (2017) proposed the lower-pressure stability of marialite to be defined by a univariant curve starting at an invariant point at 0.8 GPa and 840 °C and having a negative d*P*/d*T* curve of -0.0025 GPa/°C.

Several researchers, including Orville (1975), Ellis (1978), and Baker and Newton (1995), have done experimental work on scapolite solid solutions. Orville (1975) determined that scapolite in the system $NaAlSi_3O_8$-$CaAl_2Si_2O_8$-NaCl-$CaCO_3$ at 750 °C and 0.4 GPa is stable relative to plagioclase + calcite + halite over the approximate range of plagioclase-equivalent (= EqAn) compositions of $EqAn_{15}$ – $EqAn_{75}$, even though albite + halite is stable relative to end-member marialite and anorthite + calcite is stable relative to end-member meionite at these same conditions. It is worth noting that complete conversion of plagioclase to scapolite in the study of Orville (1975) was only attained in the presence of small amounts of water, and all experiments were seeded with small amounts of scapolite. The best growth of scapolite at the expense of

plagioclase + salts was obtained by using excess NaCl and $CaCO_3$ and trace amounts of water. Ellis (1978) determined that solid solution scapolite is stable relative to plagioclase + calcite at 750 °C and 0.4 GPa over the range of plagioclase compositions $Ab_{47}An_{53}$ to $Ab_{17}An_{83}$. This study also confirms that high mole fractions of NaCl in the fluid, as well as excess $CaCO_3$, are necessary to stabilize scapolite relative to plagioclase + NaCl + $CaCO_3$ over the widest range of scapolite compositions reported ($EqAn_{25}$ – $EqAn_{89}$). Baker and Newton (1995) investigated the stability field of scapolite, plagioclase, and calcite in the Cl-free system $CaAl_2Si_2O_8$-$NaAlSi_3O_8$-$CaCO_3$ at 775-850 °C and 0.7 GPa. Even though their study did not include NaCl, it does demonstrate that the incorporation of Na into meionite through a plagioclase coupled substitution, $NaSi(CaAl)_{-1}$ causes the expansion of the range of conditions over which scapolite is stable. It is suggested that the stabilization of meionite by substitution of Na for Ca and Si for Al is a consequence of the large amounts of atomic mixing possible in the scapolite structure and is primarily an entropy effect, as it has been previously described by Oterdoom and Gunter (1983). The results of Baker and Newton (1995) show a large stabilization of CO_3-rich scapolite to temperatures below the limit of pure meionite. Their results suggest that fifteen mole percent of sodium meionite component stabilizes scapolite by at least 70 °C (Baker and Newton, 1995).

The focus of this study is to investigate the pressure-temperature (*P*-*T*) stability of an intermediate composition scapolite of nominal bulk composition $Ma_{80}Me_{20}$ according to the proposed reaction:

$$3(Na_{0.8}Ca_{0.2})(Al_{1.2}Si_{2.8})O_8 + 0.8NaCl + 0.2CaCO_3 = (Na_{3.2}Ca_{0.8})(Al_{3.6}Si_{8.4})O_{24}(Cl_{0.8}(CO_3)_{0.2}) \quad (1)$$

plagioclase ($Ab_{80}An_{20}$) halite calcite scapolite ($Ma_{80}Me_{20}$)

with particular attention paid to any changes in the compositions of the plagioclase and scapolite along the reaction boundary. Changes in the stability of the scapolite as water is introduced to

144 the system are also investigated, where reduction in the activity of NaCl in solution is expected
145 to destabilize the scapolite. The stability field of this Cl-rich scapolite is compared to the end-
146 member scapolites and a thermodynamic model for mixing along the marialite-meionite join is
147 proposed to enable a better understanding of Cl-rich scapolite paragenesis. It will be shown that
148 subtle changes from end-member to intermediate scapolite compositions causes a dramatic
149 expansion in its stability field. This may indicate part of the reason why solid solution scapolite
150 is commonly reported in metamorphic terrains and metasomatic environments as opposed to end-
151 member scapolite, the latter not normally found in nature. End-member scapolites may simply
152 require temperature, pressure, and fluid compositions which are not normally attained or, if they
153 are attained at mid- to lower-crustal levels, may never have a chance to resurface for them to be
154 accountable in nature.

155 **Methods**

156 **Starting materials**

157 All phases were synthesized from appropriate mixtures of reagent-grade oxides, salt, and
158 carbonate (SiO_2, Al_2O_3, NaCl, Na_2CO_3, and $CaCO_3$). The SiO_2 was made by desiccating silicic
159 acid by heating gradually to 1100 °C in air overnight producing cristobalite. The reagents NaCl
160 and $CaCO_3$ were carefully brought to a temperature of at least 500 °C in air for several hours to
161 decrepitate aqueous fluid inclusions that are invariably present. After weighing and mixing the
162 reagents Na_2CO_3, $CaCO_3$, Al_2O_3, and SiO_2 constituting the framework components, they were
163 heated in air at 900 °C for 15 minutes to remove CO_2. The A-site salt components NaCl and
164 $CaCO_3$ were added following decarbonation. For hydrothermal experiments water was added in
165 the form of distilled water via a micro-syringe. The bulk compositions of all samples
166 investigated in this study are presented in Table 1.

Sample treatment and high-pressure apparatus

Starting mixtures were treated in sealed platinum and silver-palladium (Ag_{50}-Pd_{50}) capsules, which were made from tubing that was cleaned in acetone, flame-annealed to around 1,200 °C, and then crimped. Platinum capsules were used for synthesis experiments and were 4.0 mm outer diameter (OD) by 15 mm length and wall thickness of 0.18 mm. Platinum or $Ag_{50}Pd_{50}$ capsules were used for reversal experiments, depending on the conditions of treatment, and were 1.5 mm OD by 10 mm length having wall thickness of 0.13 mm. The first set of experiments focused on the synthesis of intermediate scapolite and plagioclase (i.e., $Ma_{80}Me_{20}$ and $Ab_{80}An_{20}$) and about 50-60 mg of sample was used. In subsequent reversal experiments, where all desired phases were present in a reversal mixture, about 5 mg of sample was used. For all the experiments that were treated dry, the capsules were put in a 160 °C furnace in air for 15 minutes prior to sealing to ensure that all the moisture was removed from the capsule. For hydrothermal experiments, water was introduced in the form of distilled water, as mentioned above, and the capsule was crimped shut, welded, and weighed. After completion of experiments the capsules were reweighed to check that the capsule remained sealed. To obtain a successful yield of intermediate scapolite, excess NaCl and $CaCO_3$ had to be added to the starting mixture. In order to calculate accurately the brine concentrations during the hydrothermal experiments, excess NaCl in the synthetic solid solution scapolite was rinsed in deionized water until it was completely removed from the scapolite (except reversal mixture REVSS2). The rinsed mixture was analyzed by X-ray powder diffraction to check that there was no NaCl left and then NaCl was reintroduced in known amounts to allow better accuracy in calculating brine concentrations.

A $^1/_2$-inch diameter, non-end-loaded piston-cylinder press was used for experiments with pressures at and above 1.0 GPa. Pressure media were made using NaCl outer sleeves, straight

190 graphite furnaces, and either NaCl or crushable MgO innner parts around the sample, depending
191 on the temperature. Temperatures ranged from 650 °C to 1030 °C and were measured with a
192 chromel-alumel thermocouple with the tip placed right above the sample. Temperature
193 uncertainties are estimated as ± 5 °C for reversal experiments (using smaller capsules with the
194 sample within 0.5 mm of the thermocouple tip) and ± 15 °C for synthesis experiments (using
195 larger capsules with the center of the sample within 2-3 mm of the thermocouple tip). Pressures
196 from 1.5-2.0 GPa have estimated uncertainties of 0.05 GPa. Experiments using pressure media
197 with NaCl inner parts were first pressurized to ~0.1 GPa below the desired pressure and then
198 brought to the target pressure using the thermal expansion of the assemblage, usually requiring
199 only minor bleeding off of excess pressure (hot piston-out mode). Experiments using crushable
200 MgO inner parts experienced much less thermal expansion and were therefore pressurized to the
201 desired pressure and required very little adjustment to the pressure during the heating phase.
202 Temperatures were brought up from room temperature to the target temperature using heating
203 ramps of 0.5 to 1 minute; the heating rate is noted in this study because it may have some bearing
204 on the relative nucleation rates of scapolite versus plagioclase. After treatment between 1 and 3
205 days, the piston-cylinder press was quenched and the sample retrieved. The capsule was
206 weighed, an incision was made into it, dried at 110 °C, and weighed again to determine the free-
207 water content within the capsule.
208 An internally-heated gas vessel was used for the experiments performed at pressures
209 below 1.0 GPa with argon as the pressure medium. Two Inconel®-sheathed chromel-alumel
210 thermocouples were placed in the vessel to observe any temperature gradient along the capsule;
211 gradients were generally 10 °C or less with corresponding uncertainties in the average
212 temperature of ± 5 °C. Desired temperatures were reached in 3-5 minutes. Pressures were

measured with both bourdon-tube and manganin-cell gauges and have an estimated uncertainty of 0.005 GPa. After between 2 and 6 days, the internally heated gas vessel was quenched, sample retrieved, and the water content determined following the procedures described above.

Analytical Methods

Powder X-Ray diffraction (XRD) analysis was performed using a Panalytical Xpert PW3040-MPD diffractometer. Samples were mounted on a zero-background single crystal quartz plate, with the operating settings at 40 kV and 20 mA using CuKα radiation and a diffracted-beam graphite monochromator. Samples were analyzed in a continuous scan from 10 to 60° 2Θ with a step size of 0.020° at 1.0 second per step. Reaction direction was determined using the peak-area ratios of the largest peaks of scapolite [(112), 25.8° 2Θ] and plagioclase [$(\bar{2}02)$, 27.8° 2Θ] as a simple way of estimating the proportions of these phases. The Panalytical software HighScore® was used to calculate the area of selected X-ray peaks.

Reaction-reversal starting mixtures, containing all of the desired phases, were mixed three times in an agate mortar using acetone to ensure a homogeneous mixture. Next, the mixtures were scanned from 20 to 31° 2Θ five times to acquire an average and standard deviation of the peak-area ratios for reference; reaction direction was then achieved by comparing peak-area ratios observed in subsequent treatments of the starting mixture to these reference ratios. Unit-cell dimensions were determined by Rietveld structure refinement using the program GSAS (Larson and Von Dreele, 2000). The zero point of 2Θ was refined using NaCl (a_0 = 5.6401 Å) either present in the scapolite samples or added to the plagioclase samples as an internal standard to account for differences in sample displacement from one scan to another. Refinements were initiated using the structures of albite and marialite reported by Prewitt et al. (1976) and Sokolova et al. (1996), respectively. Parameters that were refined included

background (function 1, shifted Chebyschev), scale factors, unit-cell dimensions, preferred orientation (100 axis, for halite), and LX terms in the profile function.

Electron probe micro-analysis (EPMA) was done on a JEOL 8900 Superprobe. Samples were mounted in epoxy, polished to a final diamond grit size of 0.5 μm, carbon coated, and analyzed using beam conditions of 15 kV and 10 nA. Noticeable decreases in the count rates of Na for both plagioclase and scapolite were observed after exposure to the electron beam for more than 20 s; therefore, analyses were done using 10 seconds on peaks and 3 seconds on background to minimize the effects of Na diffusion under the electron beam. No decrease in the count rates for Cl were observed for scapolite. Matrix corrections were made using the atomic number, absorption, and fluorescence (ZAF) correction scheme (e.g., Reed, 1996, p. 134–140). The standards used were: albite for Na, wollastonite for Ca, palladium chloride ($PdCl_2$) for Cl, and pure oxides for Si and Al.

Results

Synthesis and characterization of starting phases

Starting phases were synthesized in a temperature range of 700-1030 °C and 0.4-1.8 GPa for 1 to 6 days. The bulk compositions of the mixtures and synthesis conditions are listed in Table 1. In order to obtain high yields of Cl-rich scapolite three factors were considered necessary: (a) maintaining a high stoichiometric proportion of NaCl and $CaCO_3$ in the starting mixture, (b) using a relatively rapid heating time from room temperature to the target temperature (i.e., ramp time) in order to prevent plagioclase nucleation during heating, and (c) use of high temperatures. Generally, NaCl and $CaCO_3$ had to be introduced in excess to produce a substantial yield of Cl-rich scapolite (≥ 80 wt%) using ramp times of 0.5-1.0 minute (i.e., heating rates of 343-172 °C/s). Although the highest and purest yields of plagioclase were done in the internally heated

gas vessel at lower pressures under hydrothermal conditions, samples SSM1-1P and SSMF1-10, both of which were prepared with the intent to produce scapolite at 900 °C and 1.5GPa with the shorter ramp time (Table 1), yielded plagioclase along with excess halite and calcite. From this we can conclude that temperature, rather than the ramp time, played a larger role and was not sufficient to stabilize scapolite. High yields of intermediate scapolite were obtained at higher temperature conditions with longer ramp time. Generally, the synthetic scapolite and plagioclase are equant grains with average sizes being 2-5 μm, but some grains getting up to 30-50 μm in plan view, and exhibiting no apparent reaction textures (e.g., grain armoring or zonation). Figure 1a is a representative back-scattered electron image of synthetic plagioclase while Figure 1b is that of a reaction-reversal starting mixture.

Compositions of the starting material scapolite and plagioclase were obtained by electron microprobe analysis of individual grains. These data are given in Table 2 and shown as the solid symbols in Figures 2a,b. The relatively large uncertainties in the observed compositions are attributed in part to the small grain sizes and diffusion of Na under the electron beam. Despite this uncertainty, the observed average compositions of both scapolite and plagioclase are in general not the intended or nominal compositions of 0.20 mole fraction of Ca/(Ca+Na). With the exception of the plagioclase used in the higher-temperature experiments in Figure 2b (SSM1FP-4), which is within the 1σ uncertainties of the intended composition, the remainder of the starting materials are shifted to lower Ca contents. The Ca content of the plagioclase used in the lower-temperature experiments (SSM1-10) is decidedly depleted in Ca, presumably owing to the nucleation of wollastonite (Fig. 1a). Starting material scapolite (SSMF3-3, SSMF3-7) is similarly depleted in Ca which is attributed to the preferential partitioning of Ca into minor amounts of coexisting aluminosilicate and wollastonite not observed in XRD patterns but

observed under the electron microprobe. Though these compositional shifts in the starting material scapolite and plagioclase were unintended, this actually provides some means for determining whether or not compositional re-equilibration occurs in these phases during the reversal experiments, as discussed below.

To provide an independent check on the compositions of plagioclase, their compositions were estimated from the unit-cell dimension vs composition relations presented in Benesek et al. (2003) for synthetic (high) plagioclase. Of the cell dimensions given, the angle β appears to have the greatest dependence on composition. Therefore, a third-order polynomial was fit to the data of Benesek et al. (2003) for plagioclase ranging from $An_0 - An_{70}$, which is given in Table 2. Plagioclase compositions derived from this expression (Table 2) are broadly consistent with the microprobe analyses, indicating that the shifts in starting material compositions are not an artifact of the analytical technique.

The degree of Al-Si order/disorder in plagioclase for this study has been determined using the unit-cell angle γ (°) calibrated as a function of composition and Al ordering at the t_1O site by Kroll and Ribbe (1980). The degree of ordering is determined by the parameter $t_1O - \langle t_1m \rangle$, with the theoretical range of 0 to 1 for fully disordered or ordered plagioclase, respectively; however, in practice the lowest value is about 0.04 indicating the persistence of at least minor ordering in albite even after heating 40-60 d near its melting temperature (1060-1080 °C). Correction for the plagioclase composition was taken from the microprobe analyses. The observed values of $t_1O - \langle t_1m \rangle$ are given in Table 2 and range between 0.16-0.21. This indicates the presence of substantial disorder; however, its nearly constant value suggests changes in Al-Si ordering is not likely to be an important factor in the phase equilibria observed here.

Stability of Cl-rich scapolite at dry conditions

Synthesis products containing strong yields of scapolite and plagioclase were mixed together to acquire a well-seeded reversal mixture for investigating reaction (1). Thus, equilibrium is demonstrated by the growth of scapolite at the expense of plagioclase, halite, and calcite with increasing temperature and vice versa with decreasing temperature with minimum influence from phase–nucleation kinetics (Almeida and Jenkins 2017). Table 3 lists the synthesis products used to make the reversal mixtures.

A series of experiments at dry conditions was done over the range of 500-1000 °C and 0.4-2.0 GPa for 1 to 4 days. The results of these experiments are given in Table 4 and shown in Figure 3. The solid line that is shown is a straight-line interpretation of the experimental data fit "by eye." Shown for comparison is the lower-thermal stability of end-member marialite reported by Almeida and Jenkins (2017). As discussed in detail below, the compositions of the coexisting scapolite and plagioclase are $Ma_{85}Me_{15}$ and $Ab_{91}An_{09}$, respectively, indicating minor enrichment in the sodic components. What is most striking about Figure 3 is the pronounced expansion in the stability of this intermediate composition scapolite compared to end-member marialite.

Besides having a lower thermal stability, this intermediate scapolite also appears to be stable at lower pressures compared to marialite. Though limited, the lower-pressure data show that scapolite can be stable at 0.4 GPa and 750 °C as opposed to marialite that is only stable at or above 0.64 GPa. It should be noted that experiments involving mixture REVSS1 are reported in Table 4 and the results involving this mixture are broadly consistent with those obtained with mixture REVSS2. However, they were eventually not included in constructing the *P*-*T* diagram due to minor amounts of wollastonite present in this mixture, coming from the plagioclase (SSM1F-1) used in this mixture, that could possibly compromise the results near the reaction

boundary. They are included in Table 4 as supporting evidence for the placement of the univariant boundary shown in Figure 3.

Stability of Cl-rich scapolite at hydrothermal conditions

It is of interest to determine how scapolite formation is affected by the presence of water which will preferentially dissolve halite and should, at some concentration, cause scapolite to breakdown as the activity of NaCl in the ambient brine decreases. Analogous to the results reported by Almeida and Jenkins (2017) for end-member marialite, introduction of water is expected to de-stabilize the intermediate scapolite of reaction (1) as a result of the approximate reaction:

$$(Na_{3.2}Ca_{0.8})(Al_{3.6}Si_{8.4})O_{24}(Cl_{0.8}(CO_3)_{0.2}) + xH_2O = 3\ (Na_{0.8}Ca_{0.2})(Al_{1.2}Si_{2.8})O_8 + 0.2\ CaCO_3 + 0.8\ NaCl{\cdot}xH_2O\ (NaCl_l) \quad (2)$$

scapolite ($Ma_{80}Me_{20}$) water plagioclase ($Ab_{80}An_{20}$) calcite

where $NaCl_l$ is dominantly a NaCl-H_2O brine but likely with minor amounts of silicate, calcium carbonate, and water dissolved in it. This has been suggested by Eugster and Protska (1960) and supported by the study of Makhluf et al. (2016) on the system $NaAlSi_3O_8$-H_2O-NaCl at 1.0 GPa, where the latter study demonstrated at least minor (~1 wt%) albite dissolved in brines with up to 0.2 mole fraction of NaCl.

Two experiments were done with the equilibrium-reversal starting mixture REVSS2 while the remaining experiments were done with REVSS4 and REVSS5. For the latter two mixtures, any NaCl that was originally present from the scapolite synthesis was rinsed out of the samples and reintroduced in known amounts to improve the precision of the calculated brine concentrations. After rinsing samples REVSS4 and REVSS5, 4 moles of NaCl and 0.8 moles of $CaCO_3$ per mole of scapolite were added to each of them. Experiments at hydrothermal

conditions were done over the range of 660-850 °C and 1.5-2.0 GPa varying in length from 1-2 days with the results given in Table 5 and shown in Figures 4a,b. Figures 4a and 4b show the T-X_{NaCl}^{Bulk} diagrams at fixed pressures of 2.0 and 1.5 GPa, respectively, where X_{NaCl}^{Bulk} indicates the mole fraction of NaCl/(H_2O + NaCl) for the bulk mixture which may not necessarily be the true composition of the liquid phase. Because neither scapolite nor plagioclase incorporate significant amounts of water, the general configuration of Figures 4a and 4b should have a flat boundary starting at X_{NaCl}^{Bulk} = 1.0, corresponding to the location of this reaction determined from the dry experiments, and extending isothermally left to lower brine concentrations until the concentration of NaCl reaches a value where scapolite is no longer stable at this temperature. The estimated hydrothermal halite liquidus or saturation boundaries extrapolated from lower-pressure results of Aranovich and Newton (1996) are shown here for reference.

From Figures 4a,b one can see that scapolite is stable in brines as low as 0.2 X_{NaCl}^{Bulk} at 2 GPa and perhaps as low as 0.15 X_{NaCl}^{Bulk} at 1.5 GPa, though the uncertainty in the breakdown of scapolite at this pressure suggests a value as high as 0.3 as indicated by the dashed line. It appears that this intermediate composition scapolite is much more tolerant of water compared to end-member marialite. For instance, a minimum bulk salinity of 0.8 is needed at 2.0 GPa and 1050 °C to stabilize marialite (Almeida and Jenkins, 2017), which is well above the (extrapolated) halite saturation boundary at these conditions. Unlike marialite, intermediate scapolite remains stable all the way over to the halite saturation curve at 2 GPa (Fig. 4a) and near or at the saturation curve at 1.5 GPa (Fig. 4b).

The degree of order/disorder in the plagioclase formed in reaction (2) was examined for several samples which had strong plagioclase growth. Plagioclaase in REVSS4-4 treated at the higher temperature of 830 °C gave a $\Delta(131)$ value of 1.92 and γ of 89.91(2)° indicating it

remained largely disordered with corresponding values of t_1O - $\langle t_1m \rangle$ being 0.123 and 0.189, respectively. Plagioclase in REVSS5-2 grown at the lower temperature of 680 °C gave a $\Delta(131)$ value of 1.83 and γ of 89.78(2)°, both parameters giving t_1O - $\langle t_1m \rangle$ of 0.245 for $X_{An} = 0.10$. This represents a minor degree of ordering compared to the initial plagioclase (0.211), though considerably less than the nearly complete ordering ($\Delta(131) = 1.15$, t_1O - $\langle t_1m \rangle = 0.95$) expected even for pure albite at this temperature and pressure (Goldsmith and Jenkins, 1985). In general, the plagioclase has remained largely disordered and represents little change from the starting plagioclases (SSM1FP-4, SSM1-10, Table 2).

Cl-rich scapolite and plagioclase compositions

The compositions of coexisiting scapolite and plagioclase participating in reaction (2) were determined from the hydrothermal experiments, where the presence of water is expected to enhance reaction rates and promote larger grain sizes to facilitate microprobe analysis. Scapolite and plagioclase compositions from selected reversal experiments were determined via EPMA, and are listed in Tables 6 and 7, respectively.

For scapolite, the same approach for cation calculation used by Evans (1969), Lieftink et al. (1993), and Teertstra and Sherriff (1997) was applied in this study. The formula of scapolite was initially calculated by normalizing to Si + Al = 12 atoms per formula unit (apfu). The criteria for accepting the analysis was based on (1) the analytical weight-percent total from the EPMA analysis being above 80 wt%, which is well above the 65 wt% minimum determined by Giblin et al. (1993), and (2) the sum of all cations being 16.0 ± 0.2. It was difficult to obtain samples that obeyed the second criteria for the scapolite, for reasons that are unclear. One complicating factor in the microprobe analysis of marialite-rich scapolites is the rapid Na diffusion under the electron beam, even for the relatively short counting times used in this study. This diffusive loss of Na

396 under the electron beam was also described by Vanko and Bishop (1982) for the analysis of
397 marialitic scapolite. Therefore, compositions could show a slight deficit in Na and corresponding
398 relative increase in Al and Si. In an attempt to minimize Na diffusion, the current on the electron
399 microprobe was reduced to 2 nA and the analyses were done using counting times of only 3
400 seconds on peaks and 1 second on the background and using a 2 μm spot size. The analyses still
401 showed a lot of scatter; however, those analyses that adhered to the selection criteria confirmed
402 the compositions obtained under the normal higher current and longer counting times indicated
403 in the Methods section. Although the error bars are large, Figure 2a shows a systematic shift
404 from the Na-rich starting compositions (solid circles, triangle) to a composition which, on
405 average, has Ca/(Ca+Na) of 0.15 (open circles, triangle) with a corresponding scapolite
406 composition of $Ma_{85}Me_{15}$.
407 The criteria for accepting the analysis of plagioclase was based on (1) having an analytical
408 total above 80 wt% and (2) the sum of all cations were 5.0 ± 0.1 on the basis of 8 oxygens (albite
409 and anorthite equivalent to $NaAlSi_3O_8$ and $CaAl_2Si_2O_8$, respectively). Albite mole fractions
410 (X_{Ab}) were determined both by the Na-Ca ratio and Si-Al content as indicated in the footnote to
411 Table 7, and both methods were in close agreement. Figure 2b shows a systematic shift for the
412 higher-temperature experiments, which used the plagioclase SSM1FP-4 (solid square), to
413 plagioclase with slightly lower Ca contents (open squares). In contrast, the lower-temperature
414 experiment used the Ca-poor plagioclase SSM1-10 (solid diamond) which showed a slight
415 enrichment in Ca (open diamond). Taken together, the plagioclase shows an equilibrium
416 composition of about $Ab_{91}An_{09}$, which was approached from both directions.
417 Both the scapolite and plagioclase equilibrium compositions are shifted from the intended or
418 original bulk compositions of $Ma_{80}Me_{20}$ and $Ab_{80}An_{20}$, respectively. This is most noticeable for

419 the plagioclase. The deficient An content can be accounted for by the presence of minor
420 wollastonite, corundum, and quartz (Fig. 1a, Table 1) which when summed together constitute
421 anorthite. The coexistence of quartz and corundum clearly indicates that this is a metastable
422 assemblage that presumably results from the rapid nucleation of these phases relative to
423 plagioclase. Scapolite is much closer to the intended bulk composition; however, minor amounts
424 of coexisting non-scapolite phases (aluminosilicate and wollastonite, together equivalent to
425 anorthite) were observed during microprobe analysis even if they were insufficient to appear in
426 the powder XRD patterns.
427 In view of the above discussion, a more realistic representation of reaction (2) occurring in
428 the hydrothermal experiments can now be formulated that includes both the observed
429 compositional shifts in the scapolite and plagioclase as well as the minor additional phases.
430 Because the minor coexisting phases (wollastonite, aluminosilicate, etc.) can sum up to the
431 equivalent of anorthite (an_{equiv}), one can re-balance reaction (2) by allowing a certain proportion
432 of the plagioclase, up to 0.2 an_{equiv} in this case, to be exsolved as these minor phases. The
433 following reaction is balanced on the basis of one mole of scapolite of the composition
434 $Ma_{85}Me_{15}$:

435 $(Na_{3.4}Ca_{0.6})(Al_{3.45}Si_{8.55})O_{24}(Cl_{0.85}(CO_3)_{0.15}) + yH_2O = 2.8(Na_{0.91}Ca_{0.09})(Al_{1.09}Si_{2.91})O_8$ +

436 scapolite ($Ma_{85}Me_{15}$) water plagioclase ($Ab_{91}An_{09}$)

437 $(0.20 - x)(CaSiO_3+SiO_2+Al_2O_3) + 0.15CaCO_3 + [0.85NaCl \cdot x(CaSiO_3+SiO_2+Al_2O_3) \cdot yH_2O]$

438 an_{equiv} calcite $NaCl_l$ (3)

439 where the components in parentheses are the minor phases stoichiometrically equivalent to
440 anorthite (an_{equiv}) and x refers to the proportions of these components, along with y moles of
441 water, incorporated into the NaCl-rich liquid ($NaCl_l$). The stoichiometric proportions of NaCl

442 and $CaCO_3$ in reaction (3) are based on the ideal compositions of end-member marialite and
443 meionite, which, at least for NaCl, is fairly close to the average Cl content (= 0.89 ± 0.09 apfu)
444 of the scapolites reported in Table 6.

445 **Discussion**

446 **Compositions of synthetic scapolite**

447 Figure 5a shows the compositions of the synthetic scapolite (solid squares) equilibrated along
448 the univariant curve of reaction (3) as reported in Table 6. Also shown for comparison are the
449 compositions of 109 natural scapolites selected from the literature that are relatively SO_3 poor
450 and that span a wide range of scapolite-composition space. As can be seen in Figure 5a,
451 scapolite compositions do not follow any one binary end-member join. Near the Cl-rich portion
452 of this diagram, and certainly within the analytical uncertainties, the scapolites formed in this
453 study are fairly well represented by the join marialite-meionite. This choice of scapolite
454 components is also noted by Teertstra and Sherriff (1997) who, after an extensive review of the
455 literature available at that time, noted the complexity of solid solutions in the scapolites and
456 indicated two possible alternatives that may control the chemical composition of scapolites. The
457 first alternative suggests that in closed systems with a low fluid/rock ratio, variations in X_{Cl} of
458 scapolite may be preserved in metamorphic rocks on a scale of cm, suggesting that scapolite
459 composition is a sensitive indicator of NaCl activity in coexisting fluid. The second one suggests
460 that Cl content of scapolite is rather strongly controlled by the crystal structure, and that the
461 chlorinity of the coexisting fluid is a secondary factor after charge-balance constraints imposed
462 by the framework. Nonetheless, their study suggested marialite and meionite as the solid solution
463 providing the best overall representation for NaCl-rich scapolites. In view of the potential Cl
464 enrichment in the synthetic scapolite, we provide an additional plot in Figure 5b to help gauge

whether the scapolite component dipyre ($Na_3CaAl_4Si_8O_{24}Cl$) may be a significant component in the synthetic and natural Cl-rich scapolites, as trends toward the Na-rich and CO_3-free portion of the series have been reported previously. For instance, Lieftink et al. (1993) reported Cl-rich scapolites from Bamble, Norway, with 3.7 Al apfu (rather than 3.0 Al apfu, as expected for end-member marialite) for an A site fully occupied by Cl, suggesting a high proportion of the dipyre component. However, as seen in Figure 5b, there is considerable scatter of the data, even for this sampling of published scapolite analyses, making it difficult to identify any clear trend. For the purpose of the thermodynamic analysis presented below, we will adopt the marialite-meionite join as a reasonable representation of the compositional variations in scapolite, particularly at the Cl-rich end. However, we would suggest that local cation clustering, as represented by the component dipyre, may indicate that less-than-maximum cation mixing occurs which, in turn, affects the entropy and thermodynamic activity models for scapolite.

Cl-rich scapolite *P-T* phase equilibria

Results on the stability of the intermediate scapolite studied here can be compared with earlier results on end-member meionite from Newton and Goldsmith (1976) and on marialite from Almeida and Jenkins (2017) to illustrate how the addition of minor meionite affects the *P-T* stability of marialite. Figure 6 shows the lower-thermal stability of the scapolite investigated in this study ($Ma_{85}Me_{15}$) in comparison to that of the end-member scapolites marialite ($Ma_{100}Me_0$) from Almeida and Jenkins (2017) and meionite (Ma_0Me_{100}) from Newton and Goldsmith (1976). There is a pronounced expansion (~300 °C at 1.5 GPa) in the stability of scapolite arising from the 15 mol% substitution of meionite into marialite. This phenomenon is attributed to the greater entropy of mixing in scapolite relative to plagioclase. Based on the mineral analyses shown in Figure 2, there does not appear to be any obvious shift in mineral compositions along this

488 univariant boundary such that this boundary is essentially an isopleth of constant scapolite
489 composition.

490 **Marialite-meionite *T-X* phase equilibria**

491 By combining the information on the intermediate scapolite of this study with the P-T
492 stability of end-member marialite from Almeida and Jenkins (2017) and meionite from
493 Goldsmith and Newton (1977), it is possible to calculate the temperature-composition (*T-X*)
494 phase equilibria for the marialite-meionite join in equilibrium with plagioclase. The major
495 challenge in calculating a *T-X* diagram is the lack of information on the activity-composition
496 relations for scapolite and the limited experimental data to constrain any proposed activity
497 models. With this in mind, simplistic activity expressions for the Ma and Me components in
498 scapolite are used here which are sufficient to give the general configuration of the diagram, but
499 which will surely need revision as additional data become available.

500 Using an activity model involving random mixing on all sites (e.g., Price, 1985) for scapolite
501 produces activities that are dependent on the mole fraction (*X*) of site occupancy that varies as
502 X^{17} which, in turn, yields extremely small activities with attendant small differences in Gibbs
503 free energies making it challenging to calculate boundaries between coexisting phases. Instead,
504 activity expressions that involve coupled substitutions or restricted mixing arising, for example,
505 from Al avoidance in anorthitic plagioclase (e.g., Kerrick and Darken, 1975), were adopted here.
506 Based on the crystallographic study of scapolites along the marialite-meionite join by Sokolova
507 and Hawthorne (2008), the majority of cation substitution occurs on the four *T*(1) sites, which
508 range from fully occupied by Si in marialite to approximately 50% occupancy by Si and Al for
509 meionite. Assuming random mixing of Al and Si on these four *T*(1) sites and coupled

substitutions with the cations and anions in the remaining $T(2)$, M, and A sites, one has the ideal activities:

$$a_{\mathrm{Ma}}^{\mathrm{Ideal}} = X_{\mathrm{Si}}^4 = X_{\mathrm{Ma}}^4 = X^4 \quad (4a)$$

$$a_{\mathrm{Me}}^{\mathrm{Ideal}} = 4(1-X)^2\left(\frac{1+X}{2}\right)^2 \quad (4b)$$

Non-ideal mixing is accounted for using a macroscopic two-parameter (asymmetric) Margules treatment calibrated to the plagioclase and scapolite compositions from this study at 680 °C and 1.5 GPa. The associated activity coefficient γ_i for component i is calculated as:

$$RT\ln(\gamma_{\mathrm{Ma}}) = (1-X_{\mathrm{Ma}})^2[W_{\mathrm{Ma}} + 2(W_{\mathrm{Me}} - W_{\mathrm{Ma}})X_{\mathrm{Ma}}] \quad (5a)$$

$$RT\ln(\gamma_{\mathrm{Me}}) = (1-X_{\mathrm{Me}})^2[W_{\mathrm{Me}} + 2(W_{\mathrm{Ma}} - W_{\mathrm{Ms}})X_{\mathrm{Ma}}] \quad (5b)$$

where W_{Ma} and W_{Me} are the interaction parameters for the asymmetric treatment. These are multiplied by the ideal activities to obtain the real activities, i.e., $a_i = a_i^{\mathrm{Ideal}} \cdot \gamma_i$. The thermodynamic treatment of high structural state plagioclases from Newton et al. (1980) was used for the albite-anorthite join. The complete set of thermodynamic data and expressions used to calculate the *T-X* diagrams presented here is given in Appendix 1.

The calculated phase boundaries and derived values of W_{Ma} and W_{Me} calibrated to the two data points from this study at 1.5 GPa are shown in Figure 7a. Of particular note is the pronounced expansion of the scapolite stability field relative to plagioclase, similar to the *T-X* diagrams of Oterdoom and Gunter (1983) and Baker and Newton (1995) for the carbonate scapolites. The large negative interaction parameter derived in this study is also consistent with the large negative (regular solution) interaction parameters derived in the former studies.

Using the same ideal activities proposed in equations (4a,b), one can estimate interaction parameters that model, at least approximately, the T-X correlations observed for a variety of Cl-

and CO_3-rich scapolites coexisting with plagioclase as reported from different localities. Shown in Figure 7b are coexisting scapolite (solid symbols) and plagioclase (open symbols) from metamorphosed argillaceous limestones from the Chiavenna complex, Italy (Oterdoom, 1979; Oterdoom and Gunter, 1983), calc-silicate units of the Wallace Formation, northern Idaho (Rebbert and Rice, 1997), metagabbro from the Adirondack Mountains, NY (Johnson et al., 2004), and granitic gneiss from the Munali hills area of the Lufilian-Zambezi belt, Zambia (Katonga et al., 2011). Interaction parameters were derived from the approximately average compositions of coexisting plagioclase and scapolite for the Ca-poor (Cl-rich) phases, and the phase boundaries were calculated using the same thermodynamic treatment as used in Figure 7a. What is surprising is how well the Ca-rich samples are modeled by this treatment even though they were not included in deriving the interaction parameters. There are obvious inconsistencies between the boundaries modeled here and the trends shown by the field data in Figure 7b, particularly regarding the Ca-poor samples which appear to have increasing Ca contents with increasing *T*; however, the phase relations given in Figure 7b are offered as a starting point for quantifying scapolite-plagioclase phase equilibria along the marialite-meionite join.

Implications

Scapolites occur in many metamorphic terrains and metasomatic environments (Vanko and Bishop, 1982; Mora and Valley, 1989; Teertstra and Sherriff, 1997; Johnson and Barton, 2000a, 2000b; Johnson et al., 2004; Katongo et al., 2011; Hammerli et al. 2014). The overwhelming majority of scapolites are intermediate in composition (Teertstra and Sherriff, 1997) and only rarely do they approach end-member compositions, such as the Cl-rich scapolite in melt inclusions in the martian meteorite Nakhla (Filiberto et al., 2014). Understanding the *P-T-X* conditions under which Cl- and CO_3-bearing scapolite forms may help to explain the prevalence

555 of intermediate, as compared to end member, scapolites. The results from this study demonstrate
556 that a small change in the scapolite composition from end-member marialite to intermediate
557 scapolite ($Ma_{85}Me_{15}$) causes a shift in its stability, relative to the plagioclase plus salt
558 assemblage, by 260 °C from 990 ° to 730 °C at 2.0 GPa. This greatly expanded scapolite
559 stability field is illustrated in Figures 7a and 7b. Furthermore, the intermediate scapolite is much
560 more tolerant to lower brine salinities. For instance, the intermediate scapolite of this study
561 requires only a brine salinity of approximately 0.2 $X_{\mathrm{NaCl}}^{\mathrm{Bulk}}$ (near halite saturation) at 830 °C and
562 680 °C at pressures of 2.0 GPa and 1.5 GPa, respectively, in order for it to be stable. In
563 comparison, pure marialite is very intolerant to water; it requires a minimum brine salinity of
564 about 0.8 $X_{\mathrm{NaCl}}^{\mathrm{Bulk}}$ (which is *above* halite saturation) at 1050 °C and 1000 °C at pressures of 2.0
565 GPa and 1.5 GPa, respectively, to stabilize marialite. Although this experimental study was
566 mostly performed at relatively high pressures replicating lower crust conditions, one
567 experimental run (REVSS2-10) indicated that intermediate scapolite was stable at pressure as
568 low as 0.4 GPa and 750 °C. This suggests that if a closed system has an abundant source of Na
569 and Cl (i.e. evaporitic sediments or brines), marialitic scapolite could be stable at upper and
570 middle crustal conditions. Some geological settings that could contain Cl-rich scapolite at lower
571 pressure conditions are proto-oceanic rift areas, zones of back-arc spreading, or even igneous
572 intrusions into continental basins containing evaporites. The results from this study are consistent
573 with those of Ellis (1978) who found that intermediate scapolites, and not end-member marialite
574 or meionite, are stable at 750 °C and 0.4 GPa in the presence of a wide range of bulk brine
575 salinities. The combined effects of a broader thermal stability field and tolerance to lower
576 salinities mean that intermediate scapolites will be more commonly encountered in shallow- to
577 mid-crustal levels at temperatures of ~500 °C (~800 K) or higher.

Acknowledgments

The manuscript was much improved by the careful reviews of J. Filiberto and an anonymous reviewer. The authors are grateful to David Collins who assisted with the electron microprobe analyses. Financial support for this study came from NSF grant EAR-1347463 to D.M.J.

Appendix 1

The following thermodynamic expressions were used to calculate the phase diagrams shown in Figures 7a and 7b. The reactions defining the stability of the components $Na_4Al_3Si_9O_{24}Cl$ (= Ma) and $Ca_4Al_6Si_6O_{24}CO_3$ (= Me) in scapolite relative to $NaAlSi_3O_8$ (= Ab) and $CaAl_2Si_2O_8$ (=An) in plagioclase are:

$$3\ NaAlSi_3O_8 + NaCl = Na_4Al_3Si_9O_{24}Cl \qquad \text{A1}$$

$$3\ CaAl_2Si_2O_8 + CaCO3 = Ca_4Al_6Si_6O_{24}CO_3 \qquad \text{A2}$$

The equilibrium constants corresponding to these reactions are:

$$K_1 = \frac{a_{\mathrm{Ma}}^{\mathrm{Scap}}}{\left(a_{\mathrm{Ab}}^{\mathrm{Plag}}\right)^3} \qquad \text{A3}$$

$$K_2 = \frac{a_{\mathrm{Me}}^{\mathrm{Scap}}}{\left(a_{\mathrm{An}}^{\mathrm{Plag}}\right)^3} \qquad \text{A4}$$

where a_i^j is the activity of component *i* in phase *j*. Substituting the activity-composition relations indicated in equations 4a and 4b for scapolite, the activity coefficients in 5a and 5b for scapolite, and the activity-composition expressions of Newton et al. (1980) for plagioclase into A3 and A4, one has:

$$K_1 = \frac{X_{\mathrm{Ma}}^4 \cdot \gamma_{\mathrm{Ma}}}{\left(X_{\mathrm{Ab}}^2 (2 - X_{Ab}) \cdot \gamma_{\mathrm{Ab}}\right)^3} \qquad \text{A5}$$

$$K_2 = \frac{\left(4(1-X_{\mathrm{Ma}})^2\left(\frac{1+X_{\mathrm{Ma}}}{2}\right)^2\right)\cdot\gamma_{\mathrm{Ma}}}{\left((1/4)(1-X_{\mathrm{Ab}})(2-X_{Ab})^2\cdot\gamma_{\mathrm{Ab}}\right)^3} \quad \text{A6}$$

At equilibrium at a given P and T one has:

$$\Delta G_1 = 0 = \Delta G_1^{\circ} + \mathrm{R}T\ln K_1 \quad \text{A7}$$

$$\Delta G_2 = 0 = \Delta G_2^{\circ} + \mathrm{R}T\ln K_2 \quad \text{A8}$$

where ΔG is the Gibbs free energy of the reaction, $\Delta G°$ is the Gibbs free energy for the pure phases, R is the universal gas constant (kJ/K·mol), and T is temperature in Kelvins. Expressions A7 and A8 must be solved simultaneously to find the compositions of scapolite (X_{Ma}) and plagioclase (X_{Me}) that satisfy both conditions for equilibrium. Values for $\Delta G°$ were calculated using the data in Table A1 and the expression:

$$\Delta G^{\circ}_{P,T} = \Delta H^{\circ}_{1,298} - T\Delta S^{\circ}_{1,298} + \int_{298}^{T}\Delta C_P dT - T\int_{298}^{T}\left(\frac{\Delta C_P}{T}\right)dT + \Delta V^{\circ}_{1,298}(P-P_0) \quad \text{A9}$$

Table A1. Thermochemical data used in this study from Holland and Powell (2011) and from Almeida and Jenkins (2017) for marialite.

Phase	$\Delta H°_{298\mathrm{K},\,1\mathrm{bar}}$ (kJ/mol)	$S°_{298\mathrm{K},\,1\mathrm{bar}}$ (kJ/K·mol)	$V_{298\mathrm{K},\,1\mathrm{bar}}$ (kJ/kbar·mol)	a*	b (x10^5)	c	d
albite(high)	-3921.49	0.2243	10.105	0.4520	-1.3364	-1275.9	-3.9536
halite	-411.3	0.0721	2.702	0.0452	1.797	0	0
marialite	-12167.49	0.75793	33.035	1.172	9.0626	-4676.4	-8.2379
anorthite	-4232.7	0.2005	10.0790	0.3705	1.001	-4339.1	-1.961
calcite	-1207.88	0.0925	3.6890	0.1409	0.5029	-950.7	-0.858
meionite	-13842	0.752	33.9850	1.359	3.6442	-8594.7	-9.598

* The heat capacity terms (a, b, c, and d) are the coefficients in the expression $C_P = a + b(\mathrm{T}) + c/(\mathrm{T}^2) + d/(\mathrm{T}^{0.5})$, and have units that give the heat capacity (C_P) in kJ/K·mol.

References Cited

Almeida, K. M. F., and Jenkins, D. M. (2017) Stability field of the Cl-rich scapolite marialiate. American Mineralogist, 102, 2484-2493.

Aranovich, L.Y., and Newton, R.C. (1996) H_2O activity in concentrated NaCl solutions at high pressures and temperatures measured by the brucite-periclase equilibrium. Contributions to Mineralogy and Petrology, 125, 200-212.

Baker, J., and Newton, R.C. (1995) Experimentally determined activity-composition relations for Ca-rich scapolite in the system $CaAl_2Si_2O_8$-$NaAlSi_3O_8$-$CaCO_3$ at 7 kbar. American Mineralogist, 80, 744-751.

Benesek, A., Kroll, H., Cemič, L., Kohl, V., Breit, U., and Heying, B. (2003) Enthalpies in (Na,Ca)- and (K,Ca)-feldspar binaries: a high-temperature solution calorimetric study. Contributions to Mineralogy and Petrology, 145, 119-129.

Boivin, P., and Camus, G. (1981) Igneous scapolite-bearing associations in the Chaine des Puys, Massif Central (France) and Atakor (Hoggar, Algeria). Contributions to Mineralogy and Petrology, 77, 365-375.

Ellis, D.E. (1978) Stability and phase equilibria of chloride and carbonate bearing scapolites at 750°C and 4000 bar. Geochimica et Cosmochimica Acta, 42, 1271-1281.

Eugster, H.P., and Prostka, H.J. (1960) Synthetic scapolites. Geological Society of America, 71, 1859-1860.

Evans, B.W., Shaw, D.M., and Haughton, D.R. (1969) Scapolite stoichiometry. Contributions to Mineralogy and Petrology, 24, 293-305.

634 Filiberto, J., Treiman, A.H., Giesting, P.A., Goodrich, C.A., and Gross, J. (2014) High-
635 temperature chlorine-rich fluid in the martian crust: A precursor to habitability. Earth and
636 Planetary Science Letters, 401, 110-115.
637 Giblin, L.E., Blackburn, W.H., and Jenkins, D.M. (1993) X-ray continuum discrimination
638 technique for the energy dispersive analysis of fine particles. Analytical Chemistry, 65, 3576-
639 3580.
640 Goldsmith, J.R. (1976) Scapolites, granulites, and volatiles in the lower crust. Geological Society
641 of America, 87, 161-168.
642 Goldsmith, J.R., and Jenkins, D.M. (1985) The high-low albite relations revealed by reversal of
643 degree of order at high pressures. American Mineralogist, 70, 911-923.
644 Goldsmith, J. R., and Newton, R. C. (1977) Scapolite-plagioclase stability relations at high
645 pressures and temperatures in the system $NaAlSi_3O_8$-$CaAl_2Si_2O_8$-$CaCO_3$-$CaSO_4$. American
646 Mineralogist, 62, 1063-1081.
647 Graziani, G., and Lucchesi, S. (1982) The thermal behavior of scapolites. American
648 Mineralogist, 67, 1229-1241.
649 Hammerli, J., Spandler, C., Oliver, N. H. S., and Rusk, B. (2014) Cl/Br of scapolite as a fluid
650 tracer in the earth's crust: insights into fluid sources in the Mary Kathleen Fold Belt, Mt. Isa
651 Inlier, Australia. Journal of Metamorphic Geology, 32, 93-112.
652 Hammerli, J., Kemp, A. I. S., Barrett, N., Wing, B. A., Roberts, M., Arculus, R. J., Boivin, P.,
653 Nude, P. M., and Rankenburg, K., (2017) Sulfur isotope signatures in the lower crust: A
654 SIMS study on S-rich scapolite of granulites. Chemical Geology, 454, 45-66.
655 Hassan, I., and Buseck, P. R. (1988) HRTEM characterization of scapolite solid solutions.
656 American Mineralogist, 73, 119-134.

657 Holland, T. J. B., and Powell, R., 2011. An improved and extended internally consistent
658 thermodynamic dataset for phases of petrological interest, involving a new equation of state
659 for solids. Journal of Metamorphic Geology, 29, 333-383.
660 Johnson, D.A., and Barton, M.D. (2000a) Field trip day four: Buena Vista Hills, Humboldt Mafic
661 Complex, Western Nevada. Society of Economic Geologists Guidebook Series, 32, 145-162.
662 Johnson, D.A., and Barton, M.D. (2000b) Time-space development of an external brine
663 dominated, igneous-driven hydrothermal system: Humboldt mafic complex, western Nevada.
664 Society of Economic Geologists Guidebook Series, 32, 127-143.
665 Johnson, E. L., Goergen, E. T., and Fruchey, B. L. (2004) Right lateral oblique slip movements
666 followed by post-Ottawan (1050-1020 Ma) orogenic collapse along the Carthage-Colton
667 shear zone: Date from the Dana Hill metagabbro body, Adirondack Mountains, New York.
668 In: Tollo, R.P., Corriveau, L., McLelland, J., and Bartholomew, M. J. (eds) Proterozoic
669 tectonic evolution of the Grenville orogeny in North America. Boulder Colorado, Geological
670 Society of America Memoir 197, 357-378.
671 Katongo, C., Koller, F., Ntaflos, T., Koeberl, C., and Tembo, F. (2011) Occurrence and origin of
672 scapolite in the Neoproterozoic Lufilian-Zambezi belt, Zambia: Evidence/role of brine-rich
673 fluid infiltration during regional metamorphism. In: J. Ray, G. Sen, and B. Ghosh (eds)
674 Topics in Igneous Petrology, Springer Netherlands, 449-473, DOI: 10.1007/978-90-481-
675 9600-5.
676 Kerrick, D.M., and Darken, L.S. (1975) Statistical thermodynamic models for ideal oxide and
677 silicate solid solutions, with application to plagioclase. Geochimica et Cosmochimica Acta,
678 39, 1431-1442.

679 Kroll, H., and Ribbe, P. H. (1980) Determinative diagrams for Al,Si ordering in plagioclases.
680 American Mineralogist, 65, 449-457.
681 Kullerud, K., and Erambert, M. (1999) Cl-scapolite, Cl-amphibole, and plagioclase equilibria in
682 ductile shear zones at Nusfjord, Lofoten, Norway: Implications for fluid compositional
683 evolution during fluid-mineral interaction in the deep crust. Geochimica et Cosmochimica
684 Acta, 63, 3829-3844.
685 Larson, A.C., and Von Dreele, R.B. (2000) General Structure Analysis System (GSAS), Los
686 Alamos National Lab Report (LAUR) 86-748.
687 Lieftink, D.J., Nijland, T.G., and Maijer, C. (1993) Cl-rich scapolite from Odegardens Verk,
688 Bamble, Norway. Norsk Geologisk Tidsskrift, 73, 55-57.
689 Lovering, J. F., and White, A. J. R. (1964) The significance of primary scapolite in granulitic
690 inclusions from deep-seated pipes. Journal of Petrology, 5, 195-218.
691 Makhluf, A.R., Newton, R.C., and Manning, C.E. (2016) Hydrous albite magmas at lower crustal
692 pressure: new results on liquidus H_2O content, solubility, and H_2O activity in the system
693 $NaAlSi_3O_8$–H_2O–NaCl at 1.0 GPa. Contributions to Mineralogy and Petrology, 171, 75,
694 18pp, DOI 10.1007/s00410-016-1286-0.
695 Mora, C.I., and Valley, J.W. (1989) Halogen-rich scapolite and biotite: Implications for
696 metamorphic fluid-rock interaction. American Mineralogist, 74, 721-737.
697 Newton, R.C., and Goldsmith, J.R. (1976) Stability of the end-member scapolites:
698 $3NaAlSi_3O_8 \cdot NaCl$, $3CaAl_2Si_2O_8 \cdot CaCO_3$, $3CaAl_2Si_2O_8 \cdot CaSO_4$. Zeitschrift fur
699 Kristallographie, 143, 333-353.

700 Oliver, N.H.S., Wall, V.J., and Cartwright, I. (1992) Internal control of fluid compositions in
701 amphibolite-facies scapolitic calc-silicates, Mary Kathleen, Australia. Contributions to
702 Mineralogy and Petrology, 111, 94-112.
703 Orville, P.M. (1975) Stability of scapolite in the system Ab-An-NaCl-$CaCO_3$ at 4 kb and 750°C.
704 Geochimica et Cosmochimica Acta, 39, 1091-1105.
705 Oterdoom, W. H., (1979) Plagioclase-scapolite-calcite phase relations in high metamorphic
706 argillaceous limestones. Schweizerische Mineralogische und Petrographische Mitteilungen,
707 59, 417-422.
708 Oterdoom, W.H., and Gunter, W.D. (1983) Activity models for plagioclase and CO_3·scapolites –
709 An analysis of field and laboratory data. American Journal of Science, 283-A, 255-282.
710 Prewitt, C.T., Sueno, S., and Papike, J.J. (1976) The crystal structures of high albite and
711 monalbite at high temperatures. American Mineralogist, 61, 1213-1225.
712 Price, J. G. (1985) Ideal site mixing in solid solutions, with an application to two-feldspar
713 geothermometry. American Mineralogist, 70, 696-701.
714 Rebbert, C.R., and Rice, J.M. (1997) Scapolite-plagioclase exchange: Cl-CO_3 scapolite solution
715 chemistry and implications for peristerite plagioclase. Geochimica et Cosmochimica Acta,
716 61, 555-567.
717 Reed, S.J.B. (1996) Electron microprobe analysis and scanning electron microscopy in geology.
718 Cambridge University Press, Cambridge, United Kingdom.
719 Sokolova, E. and Hawthorne, F. C. (2008) The crystal chemistry of the scapolite-group minerals.
720 I. Crystal structure and long-range order. Canadian Mineralogist, 46, 1527-1554.

721 Sokolova, E.V., Kabalov, Y.K., Sherriff, B.L., Teertstra, D.K., Jenkins, D.M., Kunath-Fandrei,
722 G., Goetz, S., and Jäger, C. (1996) Marialite: Rietveld-structure refinement and ^{29}Si MAS
723 and ^{27}Al satellite transition NMR spectroscopy. Canadian Mineralogist, 34, 1039-1050.
724 Teertstra, D.K., and Sherriff, B.L. (1997) Substitutional mechanisms, compositional trends and
725 the end-member formulae of scapolite. Chemical Geology, 136, 233-260.
726 Teertstra, D. K., Schindler, M., Sherriff, B.L., and Hawthorne, F.C. (1999) Silvialite, a new
727 sulfate-dominant member of the scapolite group with an Al-Si composition near the *I*4/m-
728 $P4_2/n$ phase transition. Mineralogical Magazine, 63, 321-329.
729 Vanko, D.A., and Bishop, F.C. (1982) Occurrence and origin of marialitic scapolite in the
730 Humboldt lopolith, N.W. Nevada. Contributions to Mineralogy and Petrology, 81, 277-289.
731 Yoshino, T., and Satish-Kumar, M. (2001) Origin of scapolite in deep-seated metagabbros of the
732 Kohistan Arc, NW Himalayas. Contributions to Mineralogy and Petrology, 140, 511-531.
733
734
735

736

737 Table 1. Mixture bulk compositions, treatment conditions, and products of phase synthesis

738 experiments.

Sample Code	Bulk composition used	T (°C)	P (GPa)	t (h)	H_2O (wt%)	Products and comments
Scapolite ($Ma_{80}Me_{20}$) synthesis						
SSMF2-3	$Na_{2.4}Ca_{0.6}Al_{3.6}Si_{8.4}O_{24}$ + 6.8NaCl + 1.7$CaCO_3$	1030	1.80	23	0	scap, hal, cal
SSMF3-1	$Na_{2.4}Ca_{0.6}Al_{3.6}Si_{8.4}O_{24}$ + 6.4NaCl + 1.6$CaCO_3$	1030	1.80	23	0	scap, hal, cal
SSMF3-3	$Na_{2.4}Ca_{0.6}Al_{3.6}Si_{8.4}O_{24}$ + 6.4NaCl + 1.6$CaCO_3$	1030	1.80	20	0	scap, hal, cal, qtz
SSMF3-4	$Na_{2.4}Ca_{0.6}Al_{3.6}Si_{8.4}O_{24}$ + 6.4NaCl + 1.6$CaCO_3$	1030	1.80	20	0	scap, hal, cal, qtz
SSMF3-7	$Na_{2.4}Ca_{0.6}Al_{3.6}Si_{8.4}O_{24}$ + 6.4NaCl + 1.6$CaCO_3$	1030	1.80	20	0	scap, hal, cal
Plagioclase ($Ab_{80}An_{20}$) synthesis						
SSM1FP-1	3($Na_{0.8}Ca_{0.2}Al_{1.2}Si_{2.8}O_8$)	700	0.40	90	5.7	plag
SSM1FP-2	3($Na_{0.8}Ca_{0.2}Al_{1.2}Si_{2.8}O_8$)	700	0.40	91	7.2	glass - amorphous XRD pattern
SSM1FP-3	3($Na_{0.8}Ca_{0.2}Al_{1.2}Si_{2.8}O_8$)	700	0.40	90	2	neph, plag
SSM1-10*	3($Na_{0.8}Ca_{0.2}Al_{1.2}Si_{2.8}O_8$)	700	0.40	92	5.1	plag, cor, woll, neph
SSM1FP-4*	3($Na_{0.8}Ca_{0.2}Al_{1.2}Si_{2.8}O_8$)	700	0.40	92	5.6	plag
SSMF2-1	$Na_{2.4}Ca_{0.6}Al_{3.6}Si_{8.4}O_{24}$ + 6.8NaCl + 1.7$CaCO_3$	850	0.40	142	0	plag, hal, qtz, cal, cor
SSM1-1G	$Na_{2.4}Ca_{0.6}Al_{3.6}Si_{8.4}O_{24}$ + 1.6NaCl + 0.4$CaCO_3$	750	0.50	90	0	plag, qtz, cor, hal, cal
SSMF1G	$Na_{2.4}Ca_{0.6}Al_{3.6}Si_{8.4}O_{24}$ + 1.6NaCl + 0.4$CaCO_3$	750	0.50	90	0	plag, qtz, cor, hal, cal
SSMF3-2	$Na_{2.4}Ca_{0.6}Al_{3.6}Si_{8.4}O_{24}$ + 6.4NaCl + 1.6$CaCO_3$	800	0.55	67	0	plag, woll, scap, hal, cal
SSMF2-2	$Na_{2.4}Ca_{0.6}Al_{3.6}Si_{8.4}O_{24}$ + 6.8NaCl + 1.7$CaCO_3$	930	0.65	45	0	hal, plag, cal, cor
SSM1-1X	3($Na_{0.8}Ca_{0.2}Al_{1.2}Si_{2.8}O_8$)	800	1.00	45	0	qtz, plag, cor

SSMF1-10	$Na_{2.4}Ca_{0.6}Al_{3.6}Si_{8.4}O_{24}$ + 1.6NaCl + 0.4$CaCO_3$	900**	1.50	48	0	plag, qtz, hal, cal
SSM1-1P	$Na_{2.4}Ca_{0.6}Al_{3.6}Si_{8.4}O_{24}$ + 1.6NaCl + 0.4$CaCO_3$	900**	1.50	48	0	plag, qtz, hal, cal
SSM1F-1	3($Na_{0.8}Ca_{0.2}Al_{1.2}Si_{2.8}O_8$)	900**	1.50	45	0	plag, woll, qtz, cor

Note: Uncertainties are estimated at ± 15 °C in temperature and ± 0.05 GPa in pressure.

* Capsules were treated in the same experiment

** Heating ramp of 0.5 min used for these samples, all other at or above 1.0 GPa were 1 min

Abbreviations: cal = calcite; cor = corundum; hal = halite; neph = nepheline; plag = plagioclase; qtz = quartz; scap = scapolite; woll = wollastonite;

747 Table 2. Compositions (average of *n* analyses) and unit-cell dimensions of the starting material
748 scapolite and plagioclase used to investigate the phase-equilibria in this study.

	Scapolite			Plagioclase			
Sample	SSMF3-1	SSMF3-3	SSMF3-7	SSM1F-1	SSM1FP-1	SSM1FP-4	SSM1-10
Composition (wt%)							
n	14	16	15	12	21	16	13
SiO_2	64.3(2.1)	63.8(3.5)	66.0(3.3)	69.6(1.5)	64.5(5.2)	64.9(3.7)	67.7(3.4)
Al_2O_3	20.1(1.8)	18.0(2.5)	17.9(2.6)	19.2(0.4)	22.3(3.4)	21.6(2.2)	20.9(2.6)
CaO	2.0(1.1)	1.2(1.0)	1.4(1.1)	0.23(1.7)	3.8(3.4)	2.7(2.0)	0.6(1.0)
Na_2O	9.5(1.7)	8.2(0.9)	8.2(0.8)	10.0(0.5)	8.9(1.9)	9.2(1.1)	10.9(0.8)
Cl	4.0(0.2)	4.0(0.3)	4.2(0.3)	0.01(0.01)	na	0.00(0.01)	0.01(0.01)
Total	99.9(2.5)	95.2(5.2)	97.7(2.5)	99.0(1.7)	99.5(1.8)	98.4(2.6)	100.1(1.6)
Total-Cl=Ox	99.1(2.5)	94.4(5.2)	96.7(2.5)				
Cations per Al + Si = 12				Cations per 8 oxygens			
Si	8.80(0.25)	9.01(0.32)	9.10(0.39)	3.04(0.02)	2.85(0.19)	2.89(0.12)	2.95(0.12)
Al	3.23(0.25)	2.99(0.33)	2.90(0.39)	0.99(0.01)	1.16(0.19)	1.13(0.12)	1.07(0.14)
Ca	0.29(0.16)	0.18(0.16)	0.21(0.16)	0.01(0.01)	0.18(0.16)	0.13(0.09)	0.03(0.05)
Na	2.52(0.44)	2.26(0.24)	2.20(0.23)	0.85(0.04)	0.76(0.15)	0.79(0.08)	0.92(0.06)
Cl	0.93(0.06)	0.97(0.07)	0.98(0.08)	0.00	na	0.00	0.00
Total	15.77(0.5)	15.41(0.25)	15.39(0.29)	4.89(0.03)	4.95(0.03)	4.94(0.03)	4.97(0.05)
Ca/(Ca+Na)	0.10(0.05)	0.08(0.06)	0.09(0.06)	0.01(0.01)	0.19(0.17)	0.14(0.10)	0.03(0.05)
Unit-cell dimensions							
a (Å)	12.054(1)	12.033(1)	12.035(1)	8.1433(8)	8.1599(9)	8.1506(7)	8.1490(7)

b (Å)	12.054(1)	12.033(1)	12.035(1)	12.853(1)	12.871(2)	12.858(2)	12.855(1)
c (Å)	7.5499(8)	7.5427(8)	7.5399(7)	7.1083(6)	7.1249(7)	7.1172(6)	7.1174(5)
α (°)	90.0	90.0	90.0	93.60(1)	93.55(1)	93.58(1)	93.65(1)
β (°)	90.0	90.0	90.0	116.43(1)	116.345(9)	116.36(1)	116.46(1)
γ (°)	90.0	90.0	90.0	89.94(1)	89.92(1)	89.89(1)	89.80(1)
V (Å^3)	1096.9(2)	1092.2(2)	1092.0(2)	664.62(7)	669.01(9)	666.73(7)	665.88(6)
t_1O - $<t_1m>$*	----	----	----	0.160	0.193	0.199	0.211
An (mol%)**	----	----	----	0.4(0.8)	10.8(1.4)	8.5(1.4)	-1.7(0.5)

Note: Uncertainties (1 σ) are given in parentheses for the compositional data, and in the last digit for the unit-cell dimensions.

* Tetrahedral Al-Si ordering parameter for plagioclase from Kroll and Ribbe (1980) based on the unit-cell angle γ: 0.0 = fully disordered; 1.0 = fully ordered (all Al at t_{1O}).

** Anorthite content derived from the least-squares regression of the β (°) values for the $C\bar{1}$ plagioclase data of Benisek et al. (2003) to a 3rd-order polynomial: An (mol%) = -1.3259 X 10^9 + 3.4226 X 10^7 * β - 2.9449 X 10^5 * β^2 + 8.4464 X 10^2 * β^3

Table 3. Synthetic phases used to make reversal mixtures for reactions (1) and (2) in the text.

Reversal mixture	Scapolite	Plagioclase	Halite*	Calcite*
REVSS1	SSMF3-1	SSM1F-1	3.2 moles	0.8 moles
REVSS2	SSMF3-3	SSM1FP-1	3.2 moles	0.8 moles
REVSS4	SSMF3-3	SSM1FP-4	4 moles	0.8 moles
REVSS5	SSMF3-7	SSM1-10	4 moles	0.8 moles

* Moles of halite or calcite per mole of scapolite

762 Table 4. Treatment at dry conditions of reversal mixtures for reaction (1).

Sample code	T (°C)	P (GPa)	t (h)	Products and comments
REVSS2-15	650	0.40	70	no apparent reaction
REVSS2-10	750	0.40	96	scap, plag, hal, cal
REVSS2-12	500	1.50	44	plag, scap, hal, cal
REVSS2-16	550	1.50	46	no apparent reaction
REVSS2-17	580	1.50	46	no apparent reaction
REVSS2-14	600	1.50	46	no apparent reaction
REVSS2-18	620	1.50	46	plag, scap, hal, cal
REVSS2-19	630	1.50	23	no apparent reaction
REVSS2-11	650	1.50	45	scap, plag, hal, cal
REVSS1-6	650	2.00	44	plag, scap, hal, cal, woll
REVSS2-22	700	2.00	65	plag, scap, hal, cal
REVSS1-5	700	2.00	45	no apparent reaction
REVSS2-9	720	2.00	45	no apparent reaction
REVSS2-8	730	2.00	45	no apparent reaction
REVSS2-7	740	2.00	45	no apparent reaction
REVSS2-1	750	2.00	45	no apparent reaction
REVSS2-6	760*	2.00	45	scap, plag, hal, cal
REVSS2-4	780	2.00	47	scap, plag, hal, cal
REVSS2-5	780	2.00	66	scap, plag, hal, cal
REVSS2-3	800	2.00	22	scap, plag, hal, cal
REVSS1-4	800	2.00	22	scap, plag, hal, cal, woll

REVSS2-2	850	2.00	70	scap, plag, hal, cal
REVSS1-3	900	2.00	22	scap, hal, cal, woll
REVSS1-2	960	2.00	21	scap, hal, cal woll
REVSS1-1	1000	2.00	21	scap, hal, cal, woll

763 Note: Uncertainties are estimated as ± 5 °C in temperature and 0.05 GPa in pressure.

764 * Heating ramp of 0.5 min; all other experiments were done with a heating ramp of 1 min

765

766
767 Table 5. Treatment at hydrothermal conditions of reversal mixtures for reaction (2).

Sample code	T (°C)	P (GPa)	t (h)	H_2O (wt%)	Products and comments
REVSS5-6	660	1.50	46	~5	scap, plag, hal, cal
REVSS5-4	660	1.50	46	~12	no apparent reaction
REVSS5-5	660	1.50	44	~15	plag, hal, cal
REVSS5-3	660	1.50	47	~27	plag, scap, hal, cal, qtz
REVSS5-1	680	1.50	45.5	~16	scap, plag, hal, cal
REVSS5-2	680	1.50	45	28	plag, hal, cal
REVSS5-8	700	1.50	45	7	scap, plag, hal, cal
REVSS5-7	700	1.50	40	13	plag, hal, cal
REVSS5-10	720	1.50	47	~7	scap, plag, hal, cal
REVSS5-9	720	1.50	46	12	scap, plag, hal, cal
REVSS2-20H	800	2.00	22	3	scap, hal
REVSS4-5	800	2.0	21	10	scap, hal
REVSS4-6	800	2.0	22	17	scap, hal, cal(?)
REVSS4-7	800	2.0	23	~28	plag, hal
REVSS4-1	830	2.0	23	6	scap, hal
REVSS4-2	830	2.0	22	10	scap, plag, hal, cal
REVSS4-3	830	2.0	20	18	scap, plag, hal, cal
REVSS4-4	830	2.0	20	28	plag, hal
REVSS4-10	850	2.0	21	~7	scap, hal
REVSS4-8	850	2.0	22	~14	plag, hal, cal

REVSS4-9	850	2.00	23	~25	plag, hal, cal

Note: All experiments were done with a heating ramp of 1 min. Uncertainties are estimated as ± 5 °C in temperature and 0.05 GPa in pressure.

772 Table 6. Compositions of scapolite synthesized at hydrothermal conditions in this study, reported
773 as weight% oxides and chlorine and cations per 12 Al+Si atoms for the average of *n* electron
774 microprobe analyses. Uncertainties (1σ) are given in parentheses.

Sample	REVSS4-3	REVSS4-6	REVSS4-10	REVSS5-1
Composition (wt%)				
n	6	12	14	10
SiO_2	55.9 (6.5)	57.5 (3.8)	57.4 (4.5)	59.6 (3.8)
Al_2O_3	18.4 (2.7)	20.4 (2.1)	20.3 (1.4)	19.5 (1.8)
CaO	2.65 (1.74)	3.85 (2.04)	4.25 (2.14)	3.21 (2.37)
Na_2O	11.6 (1.7)	12.0 (2.0)	11.8 (1.5)	12.6 (1.4)
Cl	3.91 (0.64)	3.15 (0.66)	3.81 (0.47)	3.37 (0.65)
Total	92.5(10.4)	96.9(4.5)	97.6(3.8)	98.3(2.6)
Cations (per 12 Al+Si)				
TSi	8.65(0.25)	8.46(0.32)	8.46(0.30)	8.65(0.36)
TAl	3.35(0.25)	3.54(0.32)	3.54(0.30)	3.35(0.36)
Sum T	12	12	12	12
MCa	0.45(0.28)	0.61(0.33)	0.68(0.35)	0.51(0.38)
MNa	3.48(0.27)	3.41(0.31)	3.38(0.32)	3.54(0.33)
Sum M	3.93(0.12)	4.02(0.11)	4.06(0.11)	4.05(0.13)
Total	15.93(0.12)	16.02(0.11)	16.06(11)	16.05(0.13)
Anions				
Cl	1.03(0.15)	0.79(0.17)	0.96(0.13)	0.83(0.16)
Ca/(Ca+Na)	0.11(0.06)	0.15(0.05)	0.17(0.07)	0.13(0.06)

775
776
777
778
779
780
781
782
783

784

785 Table 7. Compositions of plagioclase synthesized at hydrothermal conditions in this study,
786 reported as weight% oxides and cations per 8 O atoms of the average of *n* electron microprobe
787 analyses. Uncertainties (1σ) are given in parentheses.

Sample wt%	REVSS4-4	REVSS4-7	REVSS4-8	REVSS5-2
n	9	8	6	13
SiO2	69.1(1.8)	64.5(3.3)	61.1(7.8)	67.1(3.6)
Al2O3	20.8(1.0)	19.6(1.8)	19.5(0.9)	21.0(1.5)
CaO	1.67(0.59)	1.81(1.06)	2.09(0.73)	2.08(1.16)
Na2O	11.2(0.5)	10.5(1.0)	10.3(1.3)	11.0(1.0)
Total	102.7(3.2)	96.4(5.8)	93.0(9.1)	101.3(4.7)
Cations				
TSi	2.95(0.03)	2.94(0.05)	2.89(0.09)	2.92(0.06)
TAl	1.05(0.03)	1.05(0.05)	1.09(0.09)	1.08(0.06)
Sum T	4.00	3.99	3.98	4.00
MCa	0.08(0.03)	0.09(0.05)	0.11(0.04)	0.10(0.05)
MNa	0.92(0.03)	0.92(0.05)	0.94(0.04)	0.93(0.06)
Sum M	1.00(0.03)	1.01(0.06)	1.05(0.04)	1.03(0.05)
Total	5.00(0.03)	5.01(0.06)	5.03(0.04)	5.03(0.05)
X_{Ab}*	0.92(0.02)	0.91(0.05)	0.90(0.04)	0.91(0.05)
X_{Ab}**	0.95(0.03)	0.93(0.05)	0.90(0.09)	0.90(0.04)

788 * X_{Ab} = Na/(Na+Ca)

789 ** X_{Ab} = [(2-Al)+(Si-2)]/2

790

791
792 Figure captions

793 Figure 1. Representative back-scattered-electron (BSE) images. (a) Synthetic plagioclase
794 (unlabeled grains) from sample SSM1F-1. Minor wollastonite (W) is present as the brighter
795 grains, while rare quartz (Q) can be found, though nearly identical in grey-level brightness to
796 the plagioclase. (b) Image of the reversal starting mixture REVSS1, with the larger grains
797 label accordingly as plagioclase (P), scapolite (S), quartz, and wollastonite. All but the
798 wollastonite has very similar grey-level brightness. The scapolite tends to have slightly more
799 regular blocky habit.

800 Figure 2. Compositions of starting material (solid symbols) and reaction product (open symbols)
801 phases, as determined by electron microprobe analysis, expressed in terms of the molar ratio of
802 Ca/(Ca+Na). (a) Scapolite compositions at 2.0 GPa (top) and 1.5 GPa (bottom). (b)
803 Plagioclase compositions at 2.0 GPa (top) and 1.5 GPa (bottom). Arrows indicate sense of
804 compositional re-equilibration from the starting materials (sample codes from Table 2 in
805 parentheses) to the final compositions for each of the reversal experiments indicated (REVSS
806 x-x).

807 Figure 3. *P*-*T* diagram of the experimental results of scapolite (Scap) stability (heavy solid line)
808 relative to plagioclase (Plag), halite (Hal), and calcite (Cal). Shown for comparison is the
809 stability of end-member marialite (Ma) from Almeida and Jenkins (2017, JA 17, light solid and
810 dashed lines) relative to albite (Ab) and halite, as well as the curve for end-member marialite
811 from Filiberto et al. (2014, F 14, dash-dot curve). A significant shift in stabilization has
812 occurred with the small change in chemical composition from end-member marialite to
813 intermediate scapolite of the composition $Ma_{85}Me_{15}$. Open circles indicate growth of scapolite,
814 solid circles growth of plagioclase, and half-filled circles indicate no obvious reaction. Critical

data defining the stability of end-member marialite are from Almeida and Jenkins (2017), where the solid squares represent growth of marialite and the open squares growth of albite and either halite or, at low pressure, $NaCl_{liq}$ which is a liquid rich in NaCl though not necessarily pure NaCl.

Figure 4. (a) Thermal stability of scapolite in the presence of water at 2.0 GPa, where X_{NaCl}^{Bulk} indicates the mole fraction of NaCl/(H_2O + NaCl) for the bulk mixture. Numbers indicate the (bulk) H_2O wt% used in that experiment. Estimated hydrothermal melting of NaCl ($NaCl_l$) extrapolated from lower-pressure results of Aranovich and Newton (1996). Long horizontal line is the lower-thermal stability of scapolite from Figure 3 incorporated into this diagram. (b) Stability of scapolite in the presence of water at 1.5 GPa. Possible minimum salinities of the brine before scapolite breaks down to plagioclase + calcite + liquid are shown as maximum (Max) and minimum (Min) at approximately 0.32 and 0.15 X_{NaCl}^{Bulk}, respectively. Other abbreviations and symbols as in (a).

Figure 5. (a) Chlorine contents in atoms per formula unit (apfu) vs mole fraction Ca/(Ca+Na+K) for scapolite by electron microprobe analysis of phases from this study (solid squares) and from natural samples: circles are from the Humboldt lopolith, Nevada (Vanko and Bishop, 1982; VB 1982); diamonds are from various localities reported in Graziani and Luchessi (1982; GL 1982); triangles are from the calc-silicates of the Mary Kathleen fold belt, Australia (Oliver et al.,1992; OWC 1992); dash-circles are from scapolitized metagabbros of the Bamble Sector, Norway (Lieftink et al., 1993; LNM 1993); hexagons are from scapolite-bearing calc-silicates of the Wallace Formation, Idaho (Rebbert and Rice, 1997; RR 1997); stars are scapolites from various localities (Teertstra and Sherriff, 1997; TS 1997); pluses are from a sheared gabbro-anorthosite in Lofoten, Norway (Kullerud and Erambert, 1999; KE 1999);

838 crosses are from the Dana Hill metagabbro, New York (Johnson et al., 2004; JGF 2004); and
839 squares are scapolite in a melt inclusion in the meteorite Nakhla (Filiberto et al, 2014; F et al
840 2014). Diagonal lines join ideal marialite (Ma) with mizzonite or with meionite (Me). (b)
841 Chlorine contents (apfu) vs (Si-6)/3 for synthetic and natural scapolites. Same symbols as in
842 (a). Diagonal lines join Ma and Me, mizzonite (Miz) and Ma, and Me and dipyre
843 ($Na_3CaAl_4Si_8O_{24}Cl$).
844 Figure 6. Comparison of the lower-thermal stability of the intermediate scapolite from this study
845 ($Ma_{85}Me_{15}$) with that of end-member marialite ($Ma_{100}Me_0$) from Almeida and Jenkins (2017,
846 AJ 2017) and meionite (Ma_0Me_{100}) from Goldsmith and Newton (1977, GN 1977).
847 Figure 7. (a) Calculated phase equilibria for scapolite (Scap) coexisting with albitic plagioclase
848 (Ab_{ss}) or anorthitic plagioclase (An_{ss}). Curves calculated using asymmetric or two-parameter
849 Margules treatment as discussed in the text. Interaction parameters (W_{Ma}, W_{Me}) were
850 calibrated to the two data points (circles) from this study. (b) Calculated phase equilibria as in
851 (a) but with interaction parameters calibrated to the approximate compositions of coexisting
852 Ab_{ss} and scapolite taken from the literature. Samples or compositional ranges are from
853 Oterdoom (1979 = Ot 1979, diamonds), Rebbert and Rice (1997 = RR 1997, triangles),
854 Johnson et al. (2004 = JGF 2004, squares), and Katongo et al. (2011= K et al. 2011, hexagons).
855 All assemblages are in the presence of excess halite and calcite.
856

857 Figure 1.

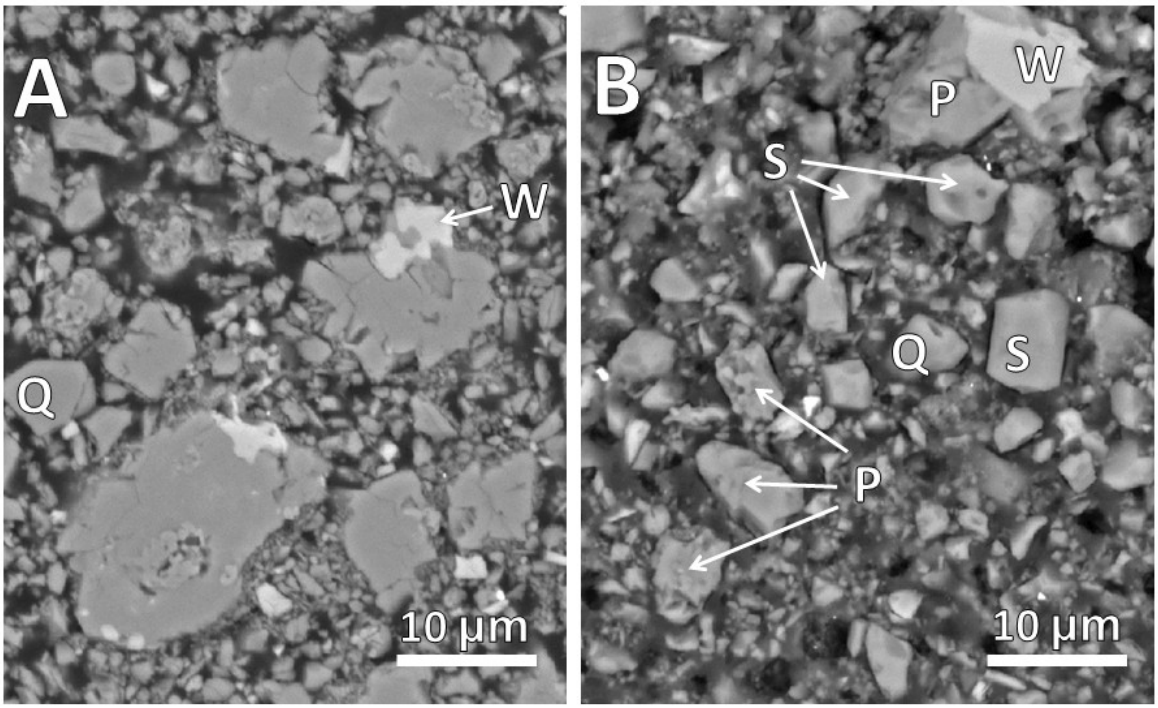

858

859 Figure 2

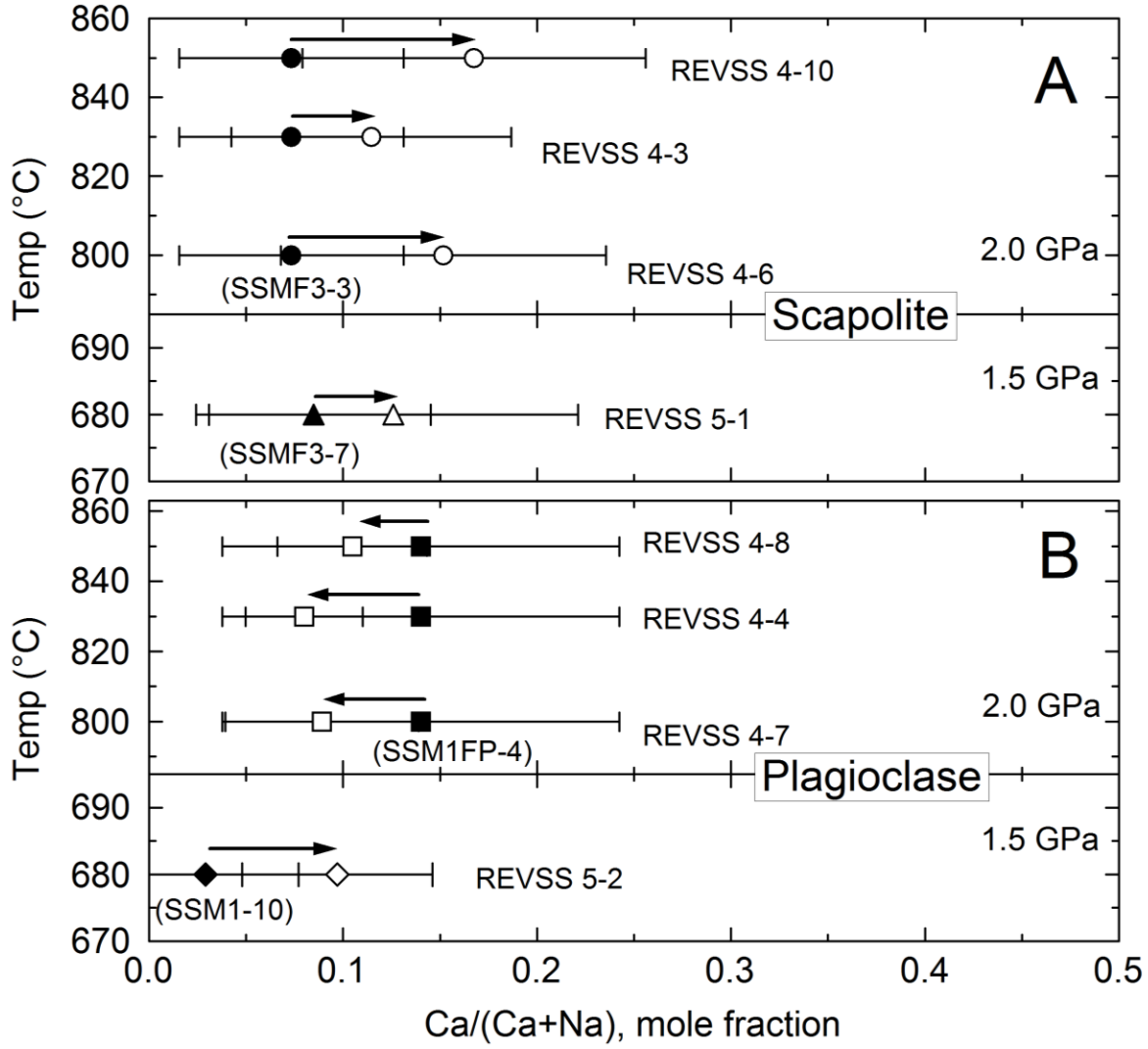

860
861
862

863 Figure 3.
864

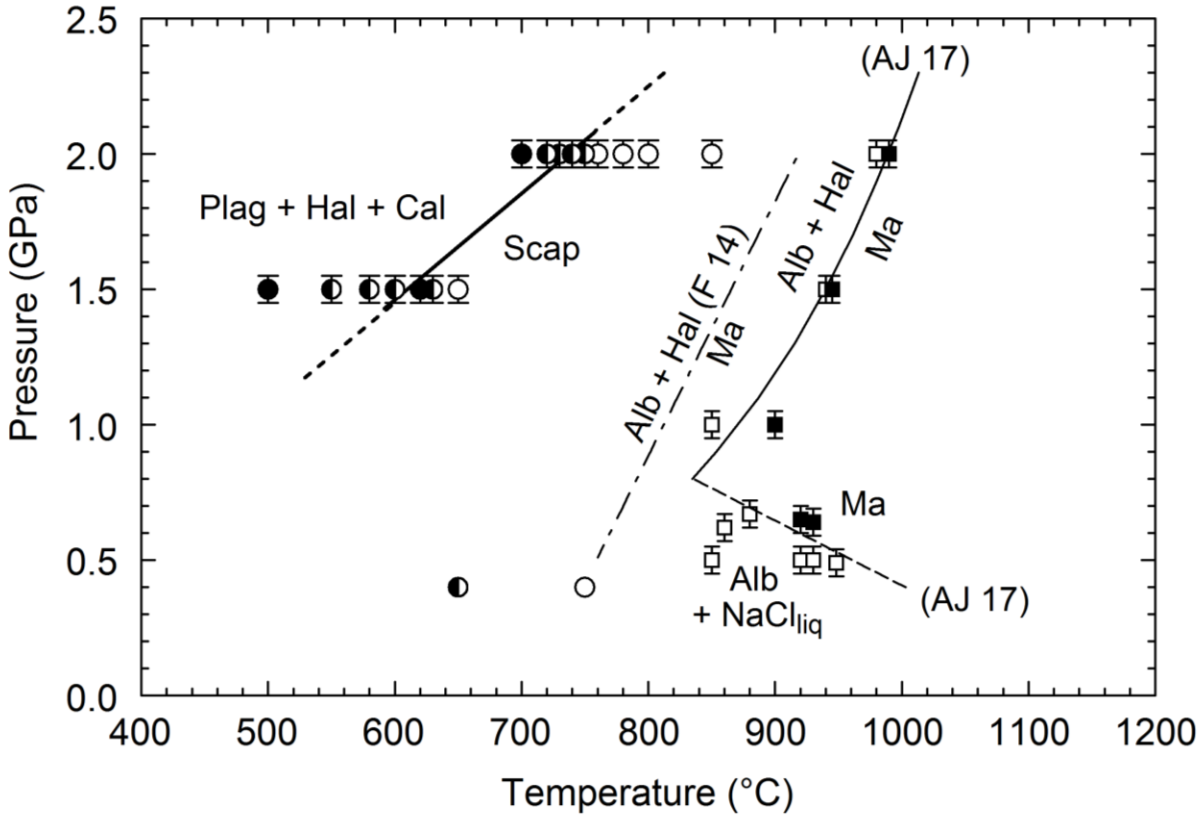

865
866
867

868
869 Figure 4. a,b

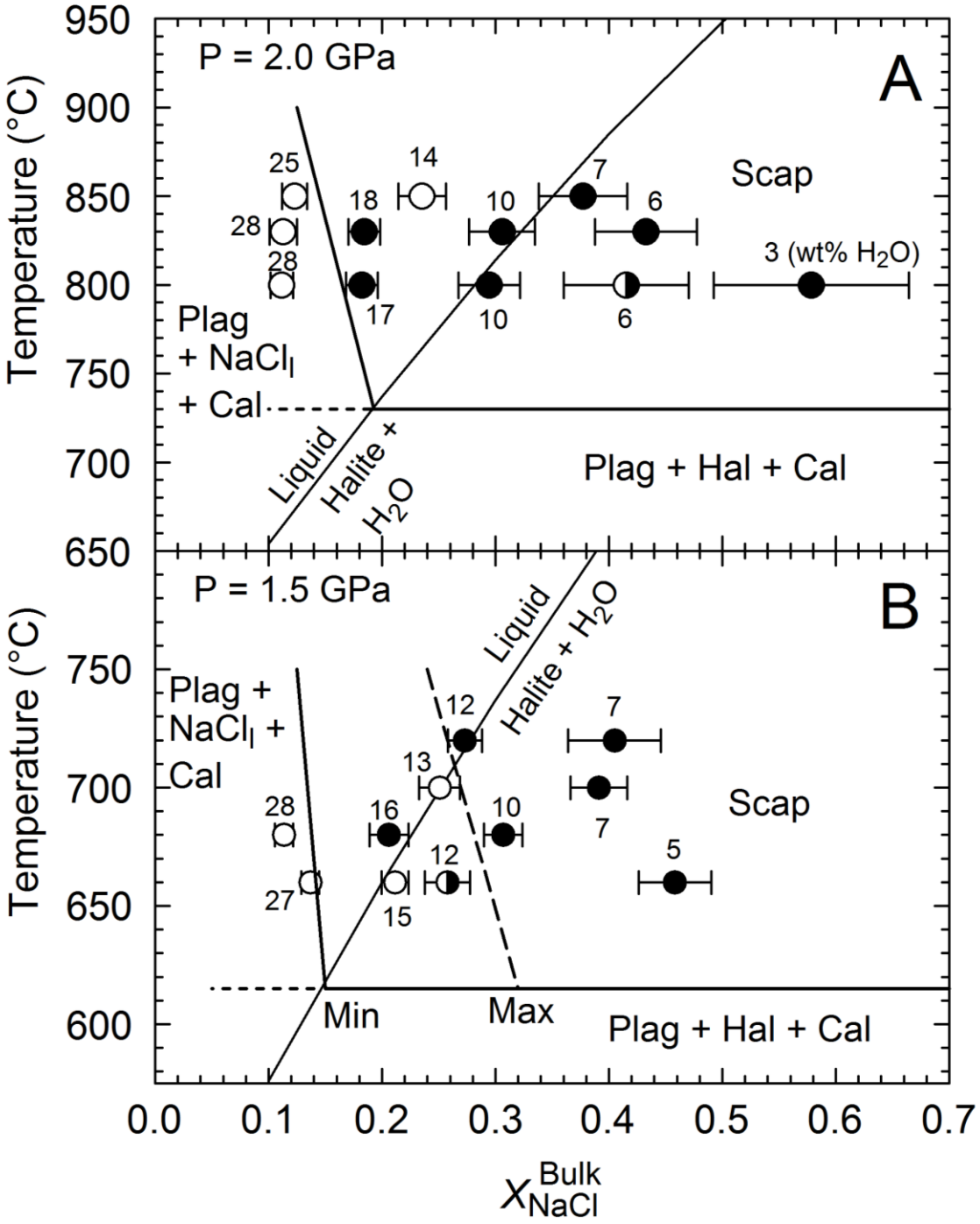

870
871
872

873 Figure 5

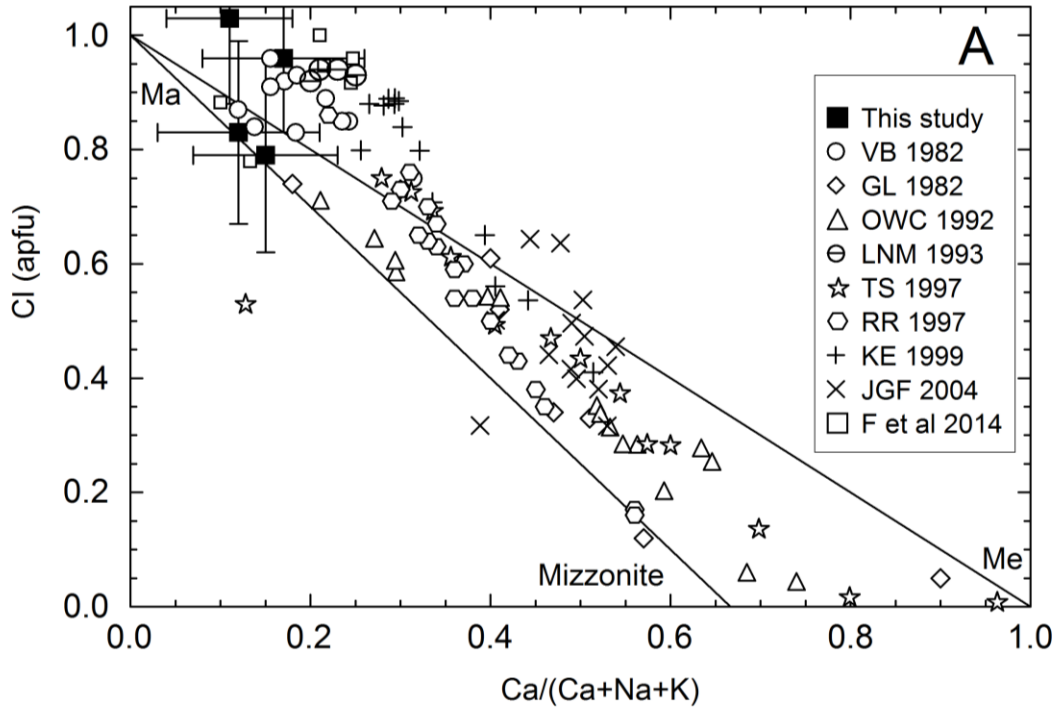

874
875

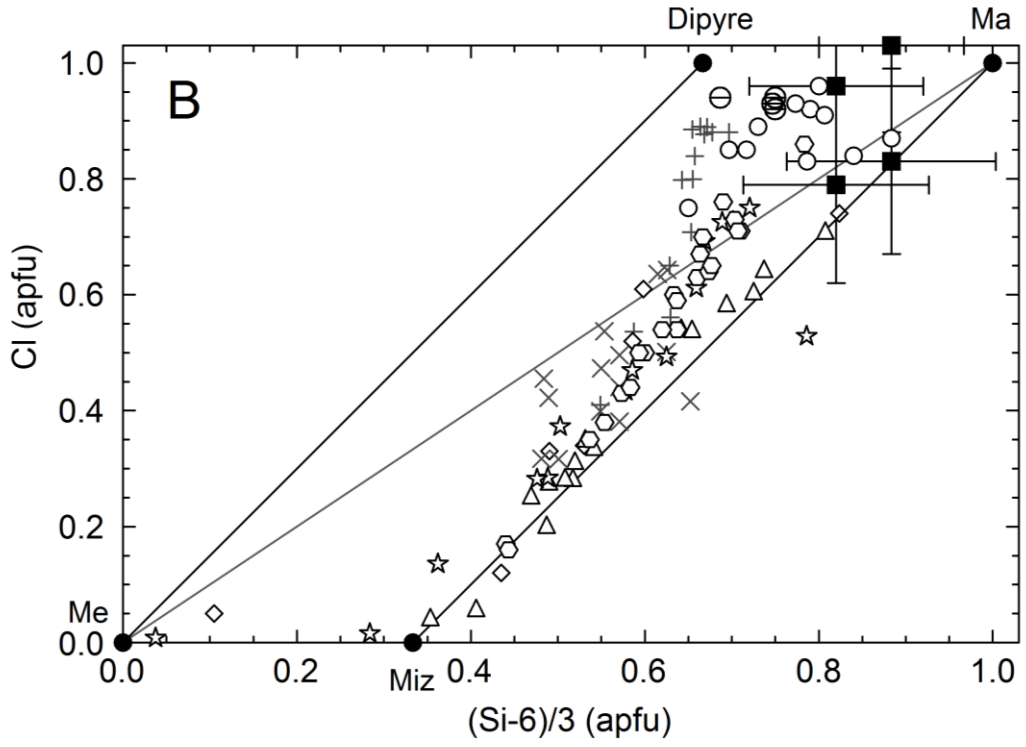

876

877
878
879 Figure 6.

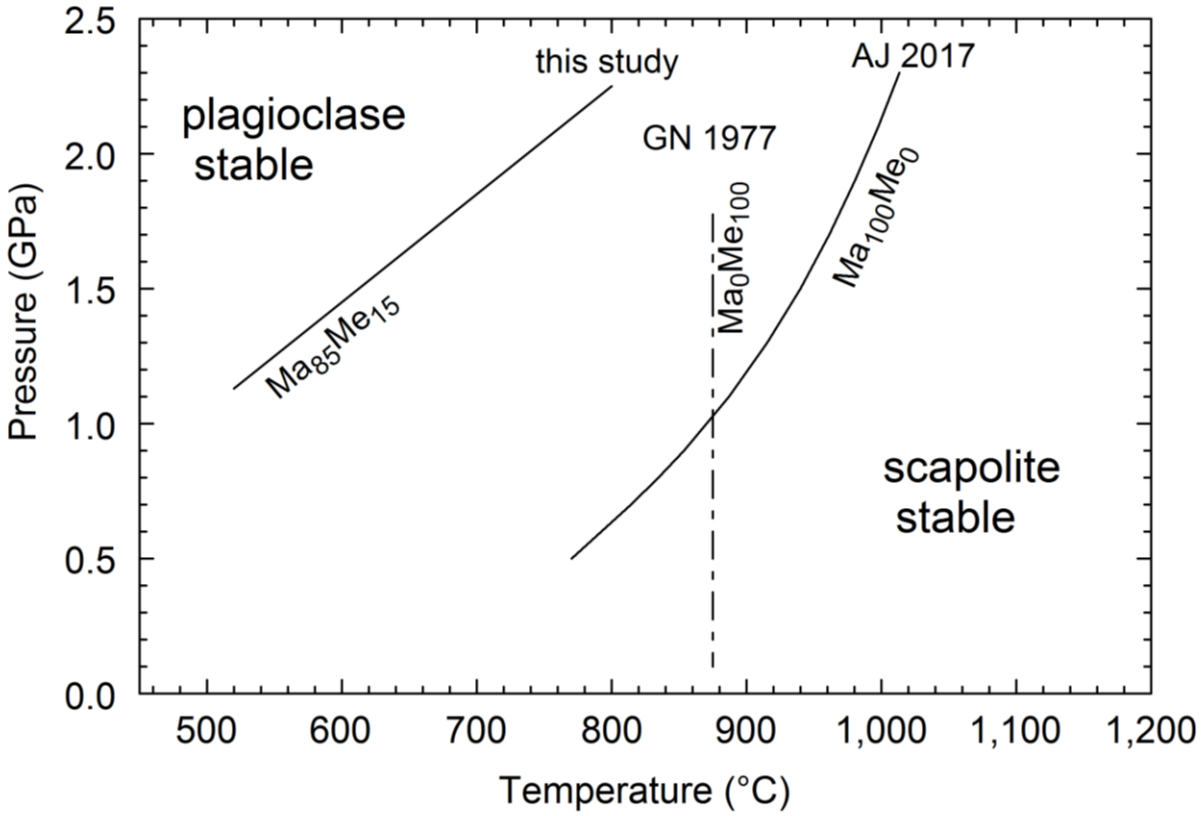

880
881

882
883
884 Figure 7.

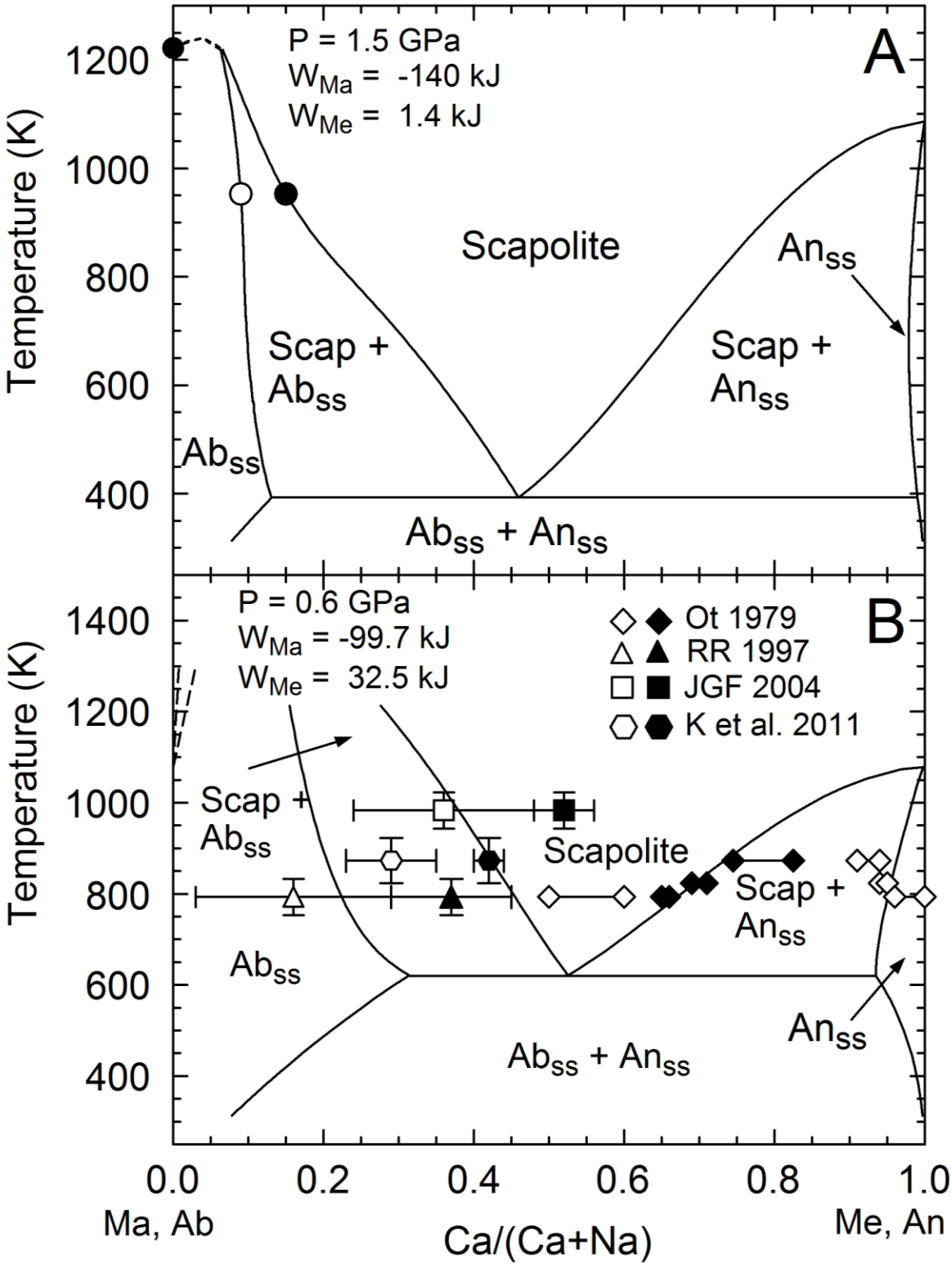

885
886